Monthly Notices
of the
ROYAL ASTRONOMICAL SOCIETY

MNRAS **447,** 1789–1805 (2015) doi:10.1093/mnras/stu2491

Wide-angle effects in future galaxy surveys

Jaiyul Yoo[1,2]★ and Uroš Seljak[1,2,3,4]

[1]*Institute for Theoretical Physics, University of Zürich, CH-8057 Zürich, Switzerland*
[2]*Lawrence Berkeley National Laboratory, University of California, Berkeley, CA 94720, USA*
[3]*Physics Department and Astronomy Department, University of California, Berkeley, CA 94720, USA*
[4]*Institute for the Early Universe, Ewha Womans University, 120-750 Seoul, South Korea*

Accepted 2014 November 25. Received 2014 October 8; in original form 2013 August 4

ABSTRACT

Current and future galaxy surveys cover a large fraction of the entire sky with a significant redshift range, and the recent theoretical development shows that general relativistic effects are present in galaxy clustering on very large scales. This trend has renewed interest in the wide-angle effect in galaxy clustering measurements, in which the distant-observer approximation is often adopted. Using the full wide-angle formula for computing the redshift-space correlation function, we show that compared to the sample variance, the deviation in the redshift-space correlation function from the simple Kaiser formula with the distant-observer approximation is negligible in galaxy surveys such as the Sloan Digital Sky Survey, *Euclid* and the BigBOSS, if the theoretical prediction from the Kaiser formula is properly averaged over the survey volume. We also find corrections to the wide-angle formula and clarify the confusion in literature between the wide-angle effect and the velocity contribution in galaxy clustering. However, when the FKP method is applied, substantial deviations can be present in the power spectrum analysis in future surveys, due to the non-uniform distribution of galaxy pairs.

Key words: methods: analytical – cosmology: observations – large-scale structure of Universe.

1 INTRODUCTION

In the past two decades, rapid experimental developments in large-scale galaxy surveys have revolutionized our understanding of the Universe such as the Sloan Digital Sky Survey (SDSS; York et al. 2000), the Two degree Field Galaxy Redshift Survey (2dFGRS; Colless et al. 2001), and the WiggleZ Dark Energy Survey (Drinkwater et al. 2010). In particular, matter fluctuations on large scales remain in the linear regime, where it is simple to relate the cosmological measurements to the governing cosmological parameters. Since two-point statistics provides a complete description of the Gaussian random field, a great deal of effort has been devoted to measuring the correlation function in configuration space and the power spectrum in Fourier space (e.g. Tegmark et al. 2004b; Cole et al. 2005; Eisenstein et al. 2005). The current state-of-the-art measurements are Reid et al. (2010) power spectrum analysis of the SDSS luminous red galaxy (LRG) samples, Blake et al. (2011b) correlation function analysis of the WiggleZ survey, and Sánchez et al. (2012) correlation function analysis of the Baryonic Oscillation Spectroscopic Survey (BOSS; Schlegel et al. 2007). Moreover, future galaxy surveys such as *Euclid*[1] and the BigBOSS[2] are planned to measure galaxies at higher redshift with larger sky coverage. With enormous statistical power in these future surveys, theoretical predictions of the redshift-space correlation function and the power spectrum need to be further refined to take full advantage of high-precision measurements.

Motivated by these recent developments, the relativistic description of galaxy clustering has been developed to meet the high accuracy of theoretical predictions demanded by these surveys (Yoo, Fitzpatrick & Zaldarriaga 2009; Yoo 2010). While measurements of galaxy clustering are based on observed quantities such as the observed redshift and the galaxy position on the sky, its theoretical prediction is based on unobservable quantities such as the real-space redshift and unlensed galaxy position. The relativistic formula for the observed galaxy fluctuation is constructed by using the observed quantities, providing a complete description of all the effects in galaxy clustering to the linear order in perturbations (Yoo et al. 2009; Yoo 2010; Bonvin & Durrer 2011; Challinor & Lewis 2011; Jeong, Schmidt & Hirata 2012). The relation between the full Kaiser formula and the relativistic formula was

★E-mail: jyoo@physik.uzh.ch

[1] http://sci.esa.int/euclid
[2] http://bigboss.lbl.gov

clarified in Yoo et al. (2012) with a careful examination of gauge issues and the Newtonian correspondence. These theoretical developments reveal that the relativistic effect is present in galaxy clustering, and the relativistic effect itself provides new opportunities to test general relativity on horizon scales in future galaxy surveys (Yoo et al. 2012).

This recent trend has renewed interest in the wide-angle effect in galaxy clustering measurements on large scales. The standard method for computing the redshift-space correlation function and its power spectrum on large scales is based on linear theory and is described by the Kaiser formula (Kaiser 1987). On large scales, where linear theory is applicable, the Kaiser formula provides a simple and physically transparent relation between the real-space $\delta_{\rm g}$ and the redshift-space $\delta_{\rm s}$ galaxy fluctuations, and its two-point correlation function (Hamilton 1992; Cole, Fisher & Weinberg 1994) or the power spectrum (Kaiser 1987) can be readily computed. This simple relation is made possible by adopting the distant-observer approximation, in which the observer is far away from galaxies in observation and hence the position angles of those galaxies are virtually identical on the sky.

Therefore, it is natural to expect this assumption to break down in wide-angle galaxy surveys, demanding a formalism for computing the redshift-space correlation function without the distant-observer approximation. When the distant-observer approximation is dropped, there exist three different angles, two lines-of-sight directions to the galaxy pair and the pair separation direction, and the resulting correlation function in redshift space is an infinite sum of plane waves with different angular momenta (see also, Fisher, Scharf & Lahav 1994; Fisher et al. 1995; Heavens & Taylor 1995; Hamilton & Culhane 1996 for the spherical power spectrum approach to redshift-space distortion). Exploiting the fact that the geometry in question is confined to a plane, Szalay, Matsubara & Landy (1998) first developed a simple expression for computing the redshift-space correlation function by using the bi-polar spherical harmonics. The wide-angle formalism is further completed in Szapudi (2004) by noting that the correlation function configuration specified by three angles can be expanded in terms of tripolar spherical harmonics and the total angular momentum of this expansion must vanish due to rotational invariance. Further extension in the wide-angle formalism was made by Matsubara (2000) to compute the correlation in a non-flat universe, by Pápai & Szapudi (2008) to implement the full Kaiser formula, by Montanari & Durrer (2012) to account for galaxy pairs at two different redshifts, and by Bertacca et al. (2012) to add relativistic corrections.

In observational side, Okumura et al. (2008) analysed the SDSS LRG sample to measure the baryonic acoustic oscillation (BAO) scale in two-dimensional redshift-space correlation function on large scales and found that the impact of the wide-angle effect on their measurements is small. Samushia, Percival & Raccanelli (2012) performed an extensive study of systematic errors in interpreting large-scale redshift-space measurements in the SDSS. By quantifying the distribution of the opening angle as a function of pair separation, they concluded that the wide angle effect is negligible in the SDSS. Beutler et al. (2011) used the 6dF Galaxy Survey for their BAO measurements by using the angle-averaged monopole correlation function. They concluded that the wide-angle effect on the monopole correlation function measurements is minor: $\Delta\xi_0^s \simeq 10^{-4}$ at the BAO scale, much smaller than the measurement uncertainties.

However, Raccanelli et al. (2013) argue that the wide-angle effect in galaxy clustering measurements is potentially degenerate with the signature of modified gravity models and it should be considered interpreting measurements in future galaxy surveys. For galaxy pairs that are widely separated in angle, the redshift-space correlation function is sufficiently different from that obtained by using the simple Kaiser formula with the distant-observer approximation, and the deviation in the correlation function measurements might be misinterpreted as the breakdown of general relativity. However, at large opening angles, where the wide-angle effect is largest, there are few galaxy pairs at a typical pair separation, and the measurement uncertainties are larger. Therefore, it is important to quantify the measurement uncertainties associated with galaxy pairs at large opening angles, and it is described by the probability distribution of the triangular shapes of galaxy pairs in each survey.

Here, we perform a systematic study of the wide angle effect in galaxy clustering measurements in galaxy surveys such as the SDSS, *Euclid* and the BigBOSS. Our results on the wide-angle effect in the SDSS agree with the previous work in Samushia et al. (2012). On the other hand, there is *no* systematic study on the wide-angle effect in future galaxy surveys. The lack of study in this direction is partially due to the difficulty in predicting measurement uncertainties in the correlation function, while various ways exist to achieve this goal when measurements are already made such as in the SDSS (see Samushia et al. 2012 for details). In contrast, it is easier to predict measurement uncertainties in the power spectrum, as each Fourier mode is independent on large scales. Therefore, our strategy is as follows. We first quantify the probability distribution of the triangular shapes formed by the observer and galaxy pairs that fit in the survey regions. The redshift-space correlation function can then be obtained by averaging each correlation function over all triangular configurations. Secondly, we compute the redshift-space power spectrum by Fourier transforming the resulting redshift-space correlation function, and we quantify the systematic errors in theoretical predictions based on the simple Kaiser formula with the distant-observer approximation by computing the covariance matrix of the redshift-space power spectrum.

Our eventual conclusion is that galaxies in surveys are sufficiently far away from the observer, and the distant-observer approximation is highly accurate. However, one has to be careful to avoid significant systematic errors when comparing theoretical predictions with measurements, because the Kaiser formula with the distant-observer approximation needs to be evaluated at a certain redshift and the deviation from the uniform distribution of cosine angle μ is substantial on large pair separations. Once these issues are properly considered in estimating the redshift-space correlation function, the systematic errors from the use of the Kaiser formula are negligible in the SDSS and are completely irrelevant in future survey. Furthermore, since the power spectrum analysis in practice is performed in a slightly different way, we investigate the systematic errors associated with the present power spectrum analysis, which turn out to be larger than the wide-angle effect.

The outline of this paper is as follows. In Section 2, the redshift-space distortion formalism is discussed. We first introduce the Kaiser formula for the redshift-space galaxy fluctuation and its power spectrum, and we present the multipole expansion and the covariance matrix. Secondly, we briefly review the wide-angle formalism for computing the redshift-space correlation function and clarify the 'wide angle effects', i.e. the deviation from the simple Kaiser formula with the distant-observer approximation. We then make connection to the full relativistic formula for the observed galaxy fluctuation and identify missing velocity corrections in the Kaiser formula and the wide-angle formalism. In Section 3, we present our main results on the systematic errors that may occur in measuring the redshift-space correlation function and the power

spectrum in the SDSS, *Euclid*, and the BigBOSS by using the simple Kaiser formula with the distant-observer approximation. Finally, we conclude in Section 4 with a discussion of our findings. For illustrations, we adopt a flat Λ cold dark matter cosmology with $\Omega_{\rm m} = 0.27$, $h = 0.703$, $n_{\rm s} = 0.966$ and $\sigma_8 = 0.809$. Throughout this paper, we only use linear theory, valid on large scales.

2 REDSHIFT-SPACE DISTORTION

Here, we briefly discuss the formalism for redshift-space distortion necessary for computing the correlation function and the power spectrum in Section 2.1 and for computing their multipole expansion and covariance matrix in Section 2.2. We then review the extension of the Kaiser formula to all sky and its deviation from the distant-observer approximation in Section 2.3 and make a connection to the full relativistic formula for the observed galaxy fluctuation in Section 2.4.

2.1 Formalism

The observed distance s of a galaxy in redshift space is based on the observed redshift z and differs from the real-space distance r due to the line-of-sight peculiar velocity V as

$$s = r + \mathcal{V} = r + f\frac{\partial}{\partial r}\nabla^{-2}\delta_m, \tag{1}$$

where the comoving line-of-sight displacement is $\mathcal{V} = V/\mathcal{H}$, the logarithmic growth rate is $f = {\rm d}\ln D/{\rm d}\ln a$, the growth factor $D(z)$ is normalized to unity at present, and the conformal Hubble parameter is $\mathcal{H} = aH$. Using the conservation of the total number of the observed galaxies in a small volume, $n_{\rm g}(s)d^3s = n_{\rm g}(r)d^3r$, the observed galaxy fluctuation $\delta_{\rm s}$ in redshift space is related to the real-space fluctuation $\delta_{\rm g}$ as

$$1 + \delta_{\rm s} = \frac{n_{\rm g}(r)}{n_{\rm g}(s)}\left|\frac{{\rm d}^3s}{{\rm d}^3r}\right|^{-1} = \frac{r^2\bar{n}_{\rm g}(r)}{s^2\bar{n}_{\rm g}(s)}\left(1 + \frac{{\rm d}\mathcal{V}}{{\rm d}r}\right)^{-1}(1 + \delta_{\rm g}). \tag{2}$$

This relation is exact but assumes that the redshift-space distortion is purely radial, ignoring angular displacements.

One can make a progress by expanding equation (2) to the linear order in perturbations, and the redshift-space galaxy fluctuation is then (Kaiser 1987)

$$\delta_{\rm s} = \delta_{\rm g} - \left(\frac{\rm d}{{\rm d}r} + \frac{\alpha}{r}\right)\mathcal{V}, \tag{3}$$

where the selection function α is defined in terms of the (comoving) mean number density $\bar{n}_{\rm g}$ of the galaxy sample as

$$\alpha \equiv \frac{{\rm d}\ln r^2\bar{n}_{\rm g}}{{\rm d}\ln r} = 2 + \frac{rH}{1+z}\frac{{\rm d}\ln\bar{n}_{\rm g}}{{\rm d}\ln(1+z)}. \tag{4}$$

By adopting the distant-observer approximation ($r \to \infty$) and ignoring the velocity contributions, a further simplification can be made (Kaiser 1987):

$$\delta_{\rm s} = b\,\delta_m - \frac{{\rm d}\mathcal{V}}{{\rm d}r} = \int\frac{{\rm d}^3\boldsymbol{k}}{(2\pi)^3}\,{\rm e}^{{\rm i}\boldsymbol{k}\cdot\boldsymbol{s}}\,(b + f\mu_k^2)\,\delta_m(\boldsymbol{k}), \tag{5}$$

where we used the linear bias approximation $\delta_{\rm g} = b\,\delta_m$ (Kaiser 1984). When we consider a fluctuation at one point such as $\delta_{\rm s}$, there are no ambiguities associated with the line-of-sight direction, and in equation (5) the cosine angle $\mu_k = \hat{\boldsymbol{s}}\cdot\hat{\boldsymbol{k}}$ between the line-of-sight direction $\hat{\boldsymbol{s}}$ and the wavevector $\boldsymbol{k}$ is always well defined, regardless of the validity of the distant-observer approximation. It is also noted that we ignore the angular displacement due to the gravitational lensing.

Under the distant-observer approximation, all galaxies are far away from the observer, and their position angles are virtually identical. In this case, equation (5) can be used to compute the power spectrum in redshift space as (Kaiser 1987)

$$P_{\rm s}(k,\mu_k) = (b + f\mu_k^2)^2 P_m(k). \tag{6}$$

Hereafter, we refer to equations (5) and (6) as the Kaiser formulae for the redshift-space galaxy fluctuation $\delta_{\rm s}$ and its power spectrum $P_{\rm s}$, but it is noted that equation (5) is the leading order terms $\sim \mathcal{O}(\delta_m)$ of the full equation (3) based on the distant-observer approximation in linear theory, and hence equation (6) $\sim \mathcal{O}(\delta_m^2)$. To separate from these 'simple' Kaiser formulae, we refer to equation (3) as the full Kaiser formula for the redshift-space galaxy fluctuation, but we explicitly spell out to distinguish the simple and the full Kaiser formulae, whenever necessary to avoid confusion.

2.2 Multipole expansion and covariance matrix

The simple Kaiser formula for the redshift-space power spectrum is anisotropic, and it is often convenient to expand $P_{\rm s}(k,\mu_k)$ in terms of Legendre polynomials $\mathcal{P}_l(x)$ as

$$P_{\rm s}(k,\mu_k) = \sum_{l=0,2,4}\mathcal{P}_l(\mu_k)P_l^s(k), \tag{7}$$

and the corresponding multipole power spectra are

$$P_l^s(k) = \frac{2l+1}{2}\int_{-1}^{1}{\rm d}\mu_k\,\mathcal{P}_l(\mu_k)P_{\rm s}(k,\mu_k). \tag{8}$$

With its simple angular structure, the simple Kaiser formula in equation (6) is completely described by three multipole power spectra

$$P_0^s(k) = \left(b^2 + \frac{2fb}{3} + \frac{f^2}{5}\right)P_m(k), \tag{9}$$

$$P_2^s(k) = \left(\frac{4bf}{3} + \frac{4f^2}{7}\right)P_m(k), \tag{10}$$

$$P_4^s(k) = \frac{8}{35}f^2P_m(k), \tag{11}$$

while any deviation from the linearity or the distant-observer approximation can give rise to higher order even multipoles ($l > 4$) and deviations of the lowest multipoles from the above equations.

The correlation function in redshift space is the Fourier transform of the redshift-space power spectrum $P_{\rm s}(k,\mu_k)$. With the distant-observer approximation the redshift-space correlation function can be computed and decomposed in terms of Legendre polynomials as

$$\xi_s(s,\mu) = \int\frac{{\rm d}^3\boldsymbol{k}}{(2\pi)^3}\,{\rm e}^{{\rm i}\boldsymbol{k}\cdot\boldsymbol{s}}\,P_{\rm s}(k,\mu_k) = \sum_{l=0,2,4}\mathcal{P}_l(\mu)\,\xi_l^s(s), \tag{12}$$

and the multipole correlation functions are related to the multipole power spectra as (Hamilton 1992; Cole et al. 1994)

$$\xi_l^s(s) = i^l\int\frac{{\rm d}k\,k^2}{2\pi^2}\,P_l^s(k)j_l(ks), \tag{13}$$

$$P_l^s(k) = 4\pi(-i)^l\int{\rm d}x\,x^2\xi_l^s(x)j_l(kx), \tag{14}$$

where $j_l(x)$ denotes the spherical Bessel functions and the cosine angle between the line-of-sight direction $\hat{\boldsymbol{n}}$ and the pair separation vector $\boldsymbol{s}$ is $\mu = \hat{\boldsymbol{n}}\cdot\hat{\boldsymbol{s}}$. With the distant-observer approximation, there

are no ambiguities associated with how to define the line-of-sight direction of the galaxy pair, as all angular directions are identical.

Due to the non-local nature of the power spectrum analysis, it is easier to handle the complex geometries of a given survey in measuring the correlation function. However, its covariance matrix is highly correlated, and more importantly measurements of the correlation function on large scales are difficult to interpret due to the non-trivial integral constraints (Peebles 1980). By contraries, the power spectrum is free from the integral constraints, and its Fourier modes are independent. Therefore, we will quantify the signal-to-noise ratios by using the redshift-space power spectrum, while we will also present our results in configuration space.

A simplest unbiased estimator of the power spectrum in redshift space is

$$\hat{P}_{\rm s}(\boldsymbol{k}) = \frac{1}{V_{\rm s}}\,\delta^s_{\boldsymbol{k}}\,\delta^s_{-\boldsymbol{k}} - \frac{1}{\bar{n}_{\rm g}}, \tag{15}$$

where $\delta^s_{\boldsymbol{k}}$ is the Fourier modes of the galaxy fluctuation in redshift space and $V_{\rm s}$ is the survey volume. To make the estimator unbiased, we subtract the shot-noise contribution due to the discrete nature of galaxies. The central limit theorem dictates that once many uncorrelated modes of the power spectrum estimates are added, the covariance matrix is well approximated by a Gaussian distribution. With the Gaussian approximation, the covariance matrix can be straightforwardly computed as (Meiksin & White 1999)

$$\begin{aligned}\mathrm{Cov}\left[\hat{P}_{\rm s}(\boldsymbol{k})\hat{P}_{\rm s}(\boldsymbol{k}')\right] &= \langle \hat{P}_{\rm s}(\boldsymbol{k})\hat{P}_{\rm s}(\boldsymbol{k}')\rangle - P_{\rm s}(\boldsymbol{k})P_{\rm s}(\boldsymbol{k}') \\ &= (\delta_{\boldsymbol{k},\boldsymbol{k}'} + \delta_{\boldsymbol{k},-\boldsymbol{k}'})\left[P_{\rm s}(k,\mu_k) + \frac{1}{\bar{n}_{\rm g}}\right]^2. \end{aligned} \tag{16}$$

Using equation (8), the covariance matrix of the multipole power spectra is (Taruya, Nishimichi & Saito 2010)

$$\begin{aligned}\mathrm{Cov}\left[\hat{P}^s{}_l(k)\hat{P}^s{}_{l'}(k')\right] &= \frac{(2l+1)(2l'+1)}{2}\,\delta_{kk'} \\ &\times \int_{-1}^{1} \mathrm{d}\mu_k\, \mathcal{P}_l(\mu_k)\mathcal{P}_{l'}(\mu_k)\left[P_{\rm s}(k,\mu_k) + \frac{1}{\bar{n}_{\rm g}}\right]^2. \end{aligned} \tag{17}$$

The covariance matrix is diagonal in Fourier modes k, but is correlated in angular multipoles l. With the redshift-space power spectrum in equation (6), the covariance matrix of the multipole power spectra can be explicitly computed and is given in Appendix A.

In the limit of highly biased objects ($\beta \to 0$), the redshift-space power spectrum becomes independent of angle, and the covariance matrix of the multipole power spectra become diagonal in angular multipole:

$$\mathrm{Cov}\left[\hat{P}^s{}_l(k)\hat{P}^s{}_{l'}(k')\right] = \delta_{kk'}\delta_{ll'}(2l+1)\left[b^2 P_m(k) + \frac{1}{\bar{n}_{\rm g}}\right]^2. \tag{18}$$

Throughout this paper, we used equation (18) to compute the intrinsic variance of the corresponding multipole power spectra and assumed that the shot-noise contribution is negligible ($\bar{n}_{\rm g} \to \infty$). Moreover, the intrinsic variance of the multipole power spectra can be further reduced by adding more measurements at each Fourier mode. Given the survey volume $V_{\rm s}$ and the galaxy number density $\bar{n}_{\rm g}$, the effective number of Fourier modes is (FKP: Feldman, Kaiser & Peacock 1994)

$$N_k = \frac{1}{2}\frac{4\pi k^2 \mathrm{d}k}{(2\pi)^3}\int \mathrm{d}V_{\rm s}\left(\frac{\bar{n}_{\rm g}P_{\rm s}}{1+\bar{n}_{\rm g}P_{\rm s}}\right)^2 \simeq \frac{1}{2}\frac{4\pi k^2 \mathrm{d}k}{(2\pi)^3}\,V_{\rm s}, \tag{19}$$

where for simplicity we assumed that the galaxy sample is limited by the sample variance, not by shot-noise. The factor 2 in equation (19) arises due to the fact that the Fourier modes represent a real quantity, i.e. the galaxy number density $n_{\rm g}$.

2.3 Redshift-space distortion in wide-angle surveys

The redshift-space correlation function without the distant-observer approximation was first computed in Szalay et al. (1998) by choosing a specific coordinate system, in which their expansion in bipolar spherical harmonics becomes particularly simple and there exist only a finite number of terms. This calculation was extended to non-flat universes (Matsubara 2000). Szapudi (2004) improved the calculation of the redshift-space correlation function by expressing it in terms of tripolar spherical harmonics, in which the expansion coefficients depend only on pair separation and only a finite number of those coefficients are present. It was shown (Szapudi 2004) that any coordinate system may be chosen to compute the redshift-space correlation, but two including the choice by Szalay et al. (1998) result in the most compact expression of the redshift-space correlation function. Further extension of the calculation was made first by Pápai & Szapudi (2008) to implement the selection function in the formula and secondly by Montanari & Durrer (2012) to account for the case where two galaxies of the pair are separated at two different redshifts.

Drawing on these previous developments, we briefly review the formalism for computing the redshift-space correlation function without the distant-observer approximation and discuss the deviation from the simple Kaiser formula with the distant-observer approximation. The full Kaiser formula for the redshift-space galaxy fluctuation in equation (3) can be recast in Fourier space as

$$\delta_{\rm s} = \int \frac{\mathrm{d}^3\boldsymbol{k}}{(2\pi)^3}\,\mathrm{e}^{\mathrm{i}\boldsymbol{k}\cdot\boldsymbol{s}}\left(b + f\mu_k^2 - \mathrm{i}\mu_k\frac{\alpha f}{k\,r}\right)\delta_m(\boldsymbol{k}), \tag{20}$$

and without adopting the distant-observer approximation the redshift-space correlation function can be formally written as

$$\begin{aligned}\xi_s &= \int \frac{\mathrm{d}^3\boldsymbol{k}}{(2\pi)^3}\,\mathrm{e}^{\mathrm{i}\boldsymbol{k}\cdot(s_1-s_2)}P_m(k|z_1,z_2)\left(b_1 + f_1\mu_{k_1}^2 - \mathrm{i}\mu_{k_1}\frac{\alpha_1 f_1}{k\,r_1}\right) \\ &\times \left(b_2 + f_2\mu_{k_2}^2 + \mathrm{i}\mu_{k_2}\frac{\alpha_2 f_2}{k\,r_2}\right), \end{aligned} \tag{21}$$

where the quantities with subscript index represent those for each galaxy of the pair, located at redshift z_1 and z_2 with angle $\hat{\boldsymbol{s}}_1$ and $\hat{\boldsymbol{s}}_2$. It is noted that with two different line-of-sight directions for each galaxy there are two different cosine angles $\mu_{k_1} = \hat{\boldsymbol{s}}_1\cdot\hat{\boldsymbol{k}}$ and $\mu_{k_2} = \hat{\boldsymbol{s}}_2\cdot\hat{\boldsymbol{k}}$, given a wavevector $\boldsymbol{k}$.

Moreover, with two galaxies on the sky, the line-of-sight direction $\hat{\boldsymbol{n}}$ of the pair can be defined in various ways. Following the lead by Szalay et al. (1998) and Szapudi (2004), we define the line-of-sight direction of the pair as the direction $\hat{\boldsymbol{n}}$, bisecting the pair in angles (hence its cosine angle $\mu_k = \hat{\boldsymbol{n}}\cdot\hat{\boldsymbol{k}}$ and $\mu = \hat{\boldsymbol{n}}\cdot\hat{\boldsymbol{s}}$, see Fig. 1 for the configuration).

In literature, the 'wide angle effects' are often used to refer to the deviation from the redshift-space power spectrum (the simple Kaiser formula) in equation (6) or the redshift-space correlation function in equation (12). Comparing equation (21) with equation (6), the deviation can be attributed to two physically distinct parts: one involves the difference among three cosine angles μ_{k_1}, μ_{k_2}, and μ_k, and the other arises from the additional velocity contribution in the full Kaiser formula that is proportional to the selection function α in equation (3). The former can be legitimately referred to as the wide-angle effect, since it represents the deviation from the one and only line-of-sight direction in the distant-observer approximation.

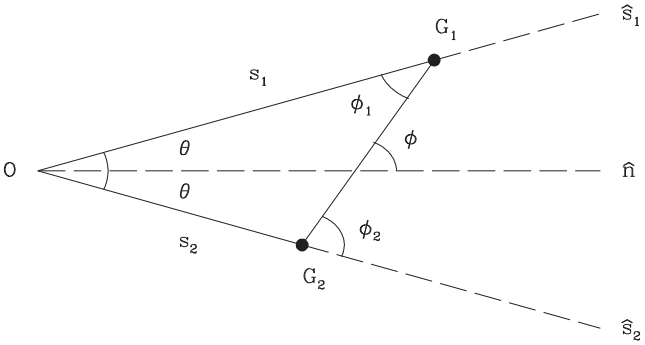

Figure 1. Triangular configuration of the observer O and the galaxy pairs G_1 and G_2. The opening angle of the galaxy pair is $\Theta \equiv 2\theta = \phi_2 - \phi_1$, and the line-of-sight direction of the pair is defined as the direction $\hat{\boldsymbol{n}}$ that bisects the pair in angle, forming an angle $\phi = (\phi_1 + \phi_2)/2$ with the pair separation. With the distant-observer approximation, three angles become identical $\phi = \phi_1 = \phi_2$ ($\theta \to 0$).

Though the latter is often referred to as the mode coupling (e.g. Raccanelli, Samushia & Percival 2010; Raccanelli et al. 2013), it just represents the additional velocity contribution, coupling the density and the velocity components, but leaving each Fourier mode uncoupled. Certainly, the latter effect is independent of how widely in angle galaxy pairs are separated. Here, we refer to the above effects as the deviation from the simple Kaiser formula with the distant-observer approximation.

Given the observed positions of the galaxy pair, $\boldsymbol{s}_1 = (\hat{\boldsymbol{s}}_1, z_1)$ and $\boldsymbol{s}_2 = (\hat{\boldsymbol{s}}_2, z_2)$, the triangular configuration formed by the galaxy pair and the observer is depicted in Fig. 1, and the redshift-space distances of the galaxy pairs and their pair separation are related as

$$s = \left[s_1^2 + s_2^2 - 2s_1 s_2 \cos\Theta\right]^{1/2}, \tag{22}$$

$$s_1 = \frac{\sin\phi_2}{\sin\Theta}\, s, \tag{23}$$

$$s_2 = \frac{\sin\phi_1}{\sin\Theta}\, s. \tag{24}$$

In Szapudi (2004), the full redshift-space correlation function in equation (21) is expanded in terms of tripolar spherical harmonics, and it is evaluated in three different coordinate systems. Following Szapudi (2004) and Pápai & Szapudi (2008), we choose a coordinate system, in which the triangle is confined in the x–y plane and the pair separation vector $\boldsymbol{s}$ is parallel to the x-axis.[3] With this choice of coordinate system, the full redshift-space correlation function can be described by a finite number of terms that depend on two angles ϕ_1, ϕ_2 and pair separation s as

$$\xi_s(s,\phi_1,\phi_2) = \sum_{i,j=0,1,2} a_{ij}(s,\phi_1,\phi_2)\cos(i\phi_1)\cos(j\phi_2) + b_{ij}(s,\phi_1,\phi_2)\sin(i\phi_1)\sin(j\phi_2), \tag{25}$$

where the coefficients non-vanishing under the distant-observer approximation are

$$a_{00} = \left(b_1 b_2 + \frac{b_2 f_1 + b_1 f_2}{3} + \frac{2 f_1 f_2}{15}\right)\xi_0^2(s) - \left(\frac{b_2 f_1 + b_1 f_2}{6} + \frac{2 f_1 f_2}{21}\right)\xi_2^2(s) + \frac{3 f_1 f_2}{140}\,\xi_4^2(s), \tag{26}$$

[3] The choice of coordinate system is, however, a matter of preference, and the resulting correlation function is independent of our choice.

$$a_{20} = -\left(\frac{b_2 f_1}{2} + \frac{3 f_1 f_2}{14}\right)\xi_2^2(s) + \frac{f_1 f_2}{28}\,\xi_4^2(s), \tag{27}$$

$$a_{02} = -\left(\frac{b_1 f_2}{2} + \frac{3 f_1 f_2}{14}\right)\xi_2^2(s) + \frac{f_1 f_2}{28}\,\xi_4^2(s), \tag{28}$$

$$a_{22} = \frac{f_1 f_2}{15}\,\xi_0^2(s) - \frac{f_1 f_2}{21}\,\xi_2^2(s) + \frac{19 f_1 f_2}{140}\,\xi_4^2(s), \tag{29}$$

$$b_{22} = \frac{f_1 f_2}{15}\,\xi_0^2(s) - \frac{f_1 f_2}{21}\,\xi_2^2(s) - \frac{4 f_1 f_2}{35}\,\xi_4^2(s), \tag{30}$$

the remaining coefficients are

$$a_{10} = \left(b_2 f_1 + \frac{2 f_1 f_2}{5}\right)\frac{\alpha_1}{r_1}\,\xi_1^1(s) - \frac{f_1 f_2}{10}\frac{\alpha_1}{r_1}\,\xi_3^1(s), \tag{31}$$

$$a_{01} = -\left(b_1 f_2 + \frac{2 f_1 f_2}{5}\right)\frac{\alpha_2}{r_2}\,\xi_1^1(s) + \frac{f_1 f_2}{10}\frac{\alpha_2}{r_2}\,\xi_3^1(s), \tag{32}$$

$$a_{11} = \frac{f_1 f_2}{3}\frac{\alpha_1\alpha_2}{r_1 r_2}\,\xi_0^0(s) - \frac{2 f_1 f_2}{3}\frac{\alpha_1\alpha_2}{r_1 r_2}\,\xi_2^0(s), \tag{33}$$

$$a_{21} = -\frac{f_1 f_2}{5}\frac{\alpha_2}{r_2}\,\xi_1^1(s) + \frac{3 f_1 f_2}{10}\frac{\alpha_2}{r_2}\,\xi_3^1(s), \tag{34}$$

$$a_{12} = \frac{f_1 f_2}{5}\frac{\alpha_1}{r_1}\,\xi_1^1(s) - \frac{3 f_1 f_2}{10}\frac{\alpha_1}{r_1}\,\xi_3^1(s), \tag{35}$$

$$b_{11} = \frac{f_1 f_2}{3}\frac{\alpha_1\alpha_2}{r_1 r_2}\,\xi_0^0(s) + \frac{f_1 f_2}{3}\frac{\alpha_1\alpha_2}{r_1 r_2}\,\xi_2^0(s), \tag{36}$$

$$b_{21} = -\frac{f_1 f_2}{5}\frac{\alpha_2}{r_2}\,\xi_1^1(s) - \frac{f_1 f_2}{5}\frac{\alpha_2}{r_2}\,\xi_3^1(s), \tag{37}$$

$$b_{12} = \frac{f_1 f_2}{5}\frac{\alpha_1}{r_1}\,\xi_1^1(s) + \frac{f_1 f_2}{5}\frac{\alpha_1}{r_1}\,\xi_3^1(s), \tag{38}$$

and we defined

$$\xi_l^n(x) = \int \frac{\mathrm{d}k}{2\pi^2}\, k^n\, j_l(kx) P_m(k|z_1, z_2), \tag{39}$$

where $P_m(k|z_1, z_2) = D(z_1)D(z_2)P_m(k|z=0)$. These coefficients are derived by extending the Pápai & Szapudi (2008) calculations to the case with two different bias factors and selection functions (Montanari & Durrer 2012). In this expansion, the redshift-space correlation function with the distant-observer approximation in equation (12) is

$$\xi_s(s,\phi) = a_{00} + a_{02}\cos 2\phi + a_{20}\cos 2\phi + a_{22}\cos^2(2\phi) + b_{22}\sin^2(2\phi). \tag{40}$$

Fig. 2 compares the full redshift-space correlation function in equation (21) to the redshift-space correlation function with the distant-observer approximation in equation (12). They are computed by using equations (25) and (40), respectively. While the latter is independent of the opening angle Θ, the former depends on the triangular configuration characterized by Θ as well as the pair separation s and the cosine angle $\mu = \cos\phi$. The upper panels show the deviation from the simple Kaiser formula with the distant-observer approximation. Panel (a) illustrates the deviation due to the wide-angle effect, in which the selection function is arbitrarily set zero $\alpha = 0$ and hence there is no velocity contribution. The deviation from the distant-observer approximation naturally becomes substantial as the opening angle increases, but it remains small at $\Theta \leq 5$ deg. With the feature in the correlation function around the BAO scale, the ratio is *not* a simple scaling of pair separation s. Panel (b) shows the full deviation from the simple Kaiser formula, including the velocity contribution. Compared to Fig. 2(a), it is apparent that the velocity contribution in this case is non-negligible,

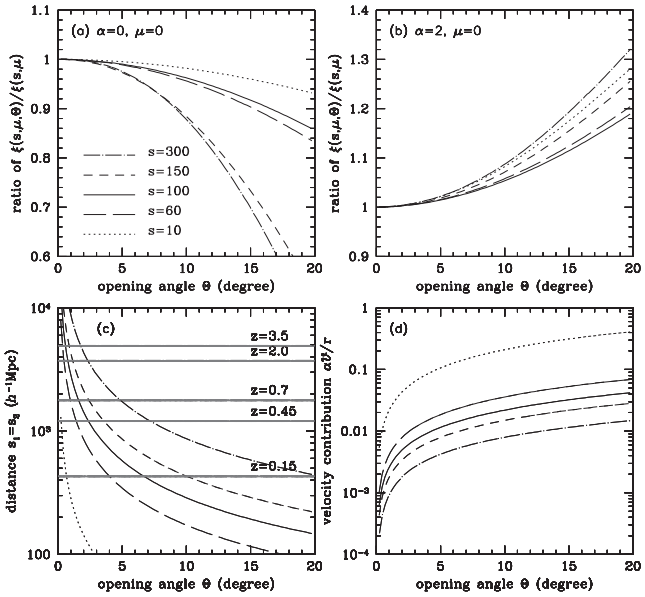

Figure 2. Full redshift-space correlation function in galaxy surveys. The full redshift-space correlation function in equation (21) depends on the triangular configuration (s, μ, Θ) formed by the galaxy pair and the observer in Fig. 1. For illustration, we consider equilateral triangular shapes (i.e. $s_1 = s_2$ and $\mu = 0$). Upper panels show the ratio of the full correlation function to the correlation function computed by using the distant-observer approximation in equation (12) at the redshift of the galaxy pair ($z_1 = z_2$). The deviation therefrom arises due to the wide-angle effect and the velocity contribution. (*a*) The selection function is set $\alpha = 0$, and there is no velocity contribution, representing the deviation purely due to the wide-angle effect. (*b*) The velocity contribution is considered ($\alpha = 2$). (*c*) The distance from the observer to each galaxy of the pair. Horizontal lines show the distance to the redshifts in the label. For reference, the SDSS LRG covers the redshift range $z = 0.15$–0.45 (*Euclid*: $z = 0.7$–2.0 and the BigBOSS: $z = 2.2 \sim 3.5$). Most galaxy pairs measured in these surveys will have small opening angles. (*d*) Approximate velocity contribution $\alpha\mathcal{V}/r$ with $V = 10^{-3}$ ($300\,\mathrm{km\,s^{-1}}$) to the full Kaiser formula for the redshift-space fluctuation δ_s in equation (3). For illustration, we assumed a uniform galaxy sample with $b = 1$ (or dark matter). Uniform galaxy samples with higher bias factor would further reduce the deviation from the distant-observer approximation.

as we explain below. In Raccanelli et al. (2010), they computed the wide-angle effect in various triangular configurations and tested the accuracy of the wide-angle formula against numerical simulations.

While the velocity contribution is independent of how widely galaxy pairs are separated in angle, the angular separation affects the velocity contribution by changing the legs of the triangle. Panel (c) shows the distance from the observer to each galaxy of the pair as a function of opening angle. With a fixed pair separation and a cosine angle, the galaxy pairs are closer to the observer as the opening angle increases. For example, the pair galaxies (solid) with $s = 100\,h^{-1}$Mpc in the equilateral configuration are about $300\,h^{-1}$Mpc away from the observer to have an opening angle of $\Theta = 10$ deg. The distances to the closer galaxy of the pairs are even closer for any triangular configuration with $\mu \neq 0$. The horizontal lines indicate redshifts at various distances, illustrating typical distances to galaxies measured in galaxy surveys. To achieve a certain number of galaxies measured in each survey, galaxy surveys are designed to cover a large cosmological volume, and galaxies in those surveys are inevitably far away from the observer. Beyond the SDSS, galaxies in surveys like *Euclid* and the BigBOSS will be at least $1\,h^{-1}$Gpc away from the observer. Consequently, the opening angles of galaxy pairs in those surveys will be a few degrees at maximum (pairs with largest separation s), and in most cases the opening angles of galaxy pairs will be close to zero.

Panel (d) shows the approximate velocity contribution term $\alpha\mathcal{V}/r$ of the full Kaiser formula δ_s for the redshift-space galaxy fluctuation in equation (3). For illustration, we assumed a typical line-of-sight velocity of $V = 10^{-3}$ ($300\,\mathrm{km\,s^{-1}}$). As the opening angle increases, the distance to galaxies decreases substantially, and this in turn increases the velocity contribution. The inverse scaling with the distance to galaxies arises due to the distortion in volume: The volume element is proportional to r^2 in the mean, and its perturbation is therefore $2\,\delta r/r \sim 2\,V/r$ with the peculiar velocity being the leading contribution to the radial distortion $\delta r \simeq |s - r|$. At a typical opening angle $\Theta \ll 1$ deg, the velocity contribution is negligible, and its contribution to the correlation function is even smaller.

2.4 Connection to the relativistic formula

The general relativistic description of galaxy clustering has been developed in the past few years (Yoo et al. 2009; Yoo 2010, see also Bonvin & Durrer 2011; Challinor & Lewis 2011; Jeong et al. 2012). The relativistic description of galaxy clustering follows the same principle as in the redshift-space distortion: the observed number of galaxies is conserved when expressed in terms of the physical and the observed quantities (Yoo 2009). In the context of redshift-space distortion, the physical quantities represent the real-space quantities, and the observed quantities represent the redshift-space quantities. However, the distinction in the physical and observed quantities is more general than in the redshift-space distortion case, and its understanding reveals the subtlety of those quantities associated with gauge issues (Yoo et al. 2009; Yoo 2010).

Observed quantities such as the observed redshift are related to physical quantities of galaxies at their rest frame by the photon geodesic equation, and perturbations along the photon path result in distortion in the observed quantities. The dominant contribution to the distortion in the observed redshift is the peculiar velocity, but there exist other relativistic contributions such as the Sachs–Wolfe and the integrated Sachs–Wolfe effects (Sachs & Wolfe 1967). Similarly, other velocity and relativistic contributions are present in the observed galaxy fluctuation due to the distortion in volume between the physical and the observed (Yoo et al. 2009; Yoo 2010).

In addition to the velocity contribution from the volume distortion, another velocity term arises in conjunction with the evolution of the source galaxy number density $\bar{n}_\mathrm{g}$, characterized by the evolution factor

$$e = 3 + \frac{\mathrm{d}\ln\bar{n}_\mathrm{g}}{\mathrm{d}\ln(1+z)}, \tag{41}$$

where the factor 3 arises due to the volume dilution and may be absorbed into $\bar{n}_\mathrm{g}$ by redefining it as the physical number density. In redshift space, the redshift-space distance s described by the observed redshift is different from the real-space distance r, and with the evolving galaxy population this mismatch gives rise to additional velocity contribution. In the conservation equation (2), this contribution is represented by the ratio of the mean number densities $\bar{n}_\mathrm{g}(r)/\bar{n}_\mathrm{g}(s)$ in real-space and redshift-space, and it is related to the selection function in the full Kaiser formula in equation (3) as

$$\alpha = \frac{\mathrm{d}\ln r^2\bar{n}_\mathrm{g}}{\mathrm{d}\ln r} = 2 + \frac{rH}{1+z}(e-3). \tag{42}$$

Apparent in its definition, the selection function α contains two physically distinct velocity contributions, by which the factor 2

represents the volume distortion and is independent of the evolving galaxy population, while the evolution factor e represents solely the distortion due to the source population. It is now evident that setting $\alpha = 0$ requires a very strange evolution of the galaxy population. A complete description of the connection between the Kaiser formula and the relativistic formula and its related gauge issues are given in Yoo et al. (2012).

In Yoo et al. (2012), we showed that while the Kaiser formula is devoid of any relativistic contribution, it properly reproduces the velocity contribution of the relativistic formula, except a missing velocity contribution from the fluctuation in the luminosity distance. Without it, the Kaiser formula can only describe galaxy samples without any selection bias, except one from the observed redshift. If galaxy samples are selected by its rest-frame luminosity, it has additional velocity contribution that is proportional to the luminosity function slope p at the threshold, and it can be implemented to the full Kaiser formula by replacing the selection function

$$\alpha \to \alpha_{\rm full} \equiv \alpha + 5p\,(\mathcal{H}r - 1), \tag{43}$$

where the luminosity function slope is

$$p = \frac{{\rm d}\log\bar{n}_{\rm g}}{{\rm d}M} = -0.4\,\frac{{\rm d}\log\bar{n}_{\rm g}}{{\rm d}\log L}, \tag{44}$$

and the absolute magnitude and luminosity are M and L, respectively.

Furthermore, the mapping between the real-space and the redshift-space takes place through the past light cone, as we observe galaxies by measuring photons. In other words, galaxies at higher redshift are not only farther away from the observer, but also farther back in time. This implies the derivative term in the full Kaiser formula for the redshift-space galaxy fluctuation in equation (3) is the total derivative along the photon path:

$$\frac{\rm d}{{\rm d}r} = \frac{\partial}{\partial r} - \frac{\partial}{\partial\tau}, \tag{45}$$

where τ is the conformal time. It is only with this relation that the full Kaiser formula in equation (3) reproduces the complete velocity terms in the relativistic formula. With the additional correction in equation (43) due to the fluctuation in the luminosity distance, the full Kaiser formula for the redshift-space galaxy fluctuation is (Yoo et al. 2012)

$$\begin{aligned}\delta_z &= b\,\delta_m - \left(\frac{\rm d}{{\rm d}r} + \frac{\alpha_{\rm full}}{r}\right)\mathcal{V}\\ &= b\,\delta_m - \frac{1+z}{H}\frac{{\rm d}V}{{\rm d}r} - e\,V + 2\,V - \frac{2V}{\mathcal{H}r}\\ &\quad + \frac{1+z}{H}\frac{{\rm d}H}{{\rm d}z}\,V - 5p\left(1 - \frac{1}{\mathcal{H}r}\right)V.\end{aligned} \tag{46}$$

Again, we emphasize that in addition to the velocity contribution in equation (46) there exist additional relativistic contributions (Yoo et al. 2009, 2012; Yoo 2010). The relativistic contributions are smaller than the velocity contributions, and they are omitted here for simplicity.

The observation that the derivative from the Jacobian in equation (2) is the total derivative reveals the mistakes made in the Kaiser formulae in equations (5) and (20) in Fourier space and hence its correlation function in equation (21). In all those cases, the derivative term is regarded as a partial derivative in space, which is sensible in equation (5) when only the leading contribution $\sim \mathcal{O}(\delta)$ is considered. However, when the velocity terms are considered as in equations (20) and (21), the time derivative should be considered in order to fully recover the velocity terms in equation (46):

$$\begin{aligned}-\frac{{\rm d}\mathcal{V}}{{\rm d}r} &= -\frac{1+z}{H}\frac{{\rm d}V}{{\rm d}r} - V + \frac{1+z}{H}\frac{{\rm d}H}{{\rm d}z}\,V\\ &= \int\frac{{\rm d}^3\boldsymbol{k}}{(2\pi)^3}\left[f\mu_k^2\delta_k - \frac{i\mu_k}{\mathcal{H}}\left(v_k' - \mathcal{H}v_k + \frac{{\rm d}H}{{\rm d}z}\,v_k\right)\right]{\rm e}^{{\rm i}\boldsymbol{k}\cdot\boldsymbol{s}},\end{aligned} \tag{47}$$

where $V_k = -i\mu_k v_k$. Consequently, the full redshift-space correlation function in equation (21) and the following equations (31)–(38) are affected by the missing velocity contributions from the time derivative. Therefore, it is noted that the velocity contribution is in fact non-vanishing, even when $\alpha_{\rm full} = 0$ (or $\alpha = 0$) or the distant-observer approximation is adopted. These corrections can be made to those equations in Fourier space, simply by replacing the selection function

$$\alpha_{\rm full} \to \alpha_{\rm full} + \mathcal{H}r - r\,\frac{{\rm d}H}{{\rm d}z}, \tag{48}$$

where the time derivative v_k' of velocity is ignored, consistently as other gravitational potential contributions. Note, however, that while equation (48) accounts for the fact that equations (5) and (20) (and hence the coefficients in equations 31–38) incorrectly compute the total derivative in Fourier space, the selection function $\alpha_{\rm full}$ in equation (43) is correct.

3 RESULT

3.1 Survey geometry

Having established the formulae for computing the redshift-space galaxy clustering and its associated error bars, we are now in a position to quantify the deviation of galaxy clustering measurements in galaxy surveys from the simple Kaiser formula with the distant-observer approximation. Here, we consider the simplest survey geometry, in which the survey area is a single contiguous region, fully characterized by its sky coverage $f_{\rm sky}$ and redshift range. For simplicity, we assume that the angular selection function is unity within the survey region, and there are no holes in the survey region. In practice, survey regions are a sum of disconnected patches on the sky (e.g. York et al. 2000; Colless et al. 2001). Moreover, each patch often contains numerous holes and is described by non-trivial angular selection function, all of which discourage observers from measuring galaxy clustering at a large separation (see, however, Lynden-Bell 1971 for likelihood methods in these cases). Surveys are often designed to have contiguous patches of size at best somewhat larger than the BAO scale (e.g. York et al. 2000; Schlegel et al. 2007; Blake et al. 2010), but significantly larger patches are in practice difficult to construct in the current generation of surveys. Therefore, our simplified geometry will maximize the deviation from the simple Kaiser formula with the distant-observer approximation by allowing widely separated galaxy pairs to be used for measuring galaxy clustering that are often unavailable in realistic galaxy surveys.

The radial selection function is the expected number density of galaxies, or the unclustered mean number density. In general, the mean galaxy number density $\bar{n}_{\rm g}(z)$ is obtained by averaging the observed galaxy number density over the survey area given redshift bins, and hence it is subject to the sample variance error. Further complication arises due to the way the galaxy sample is defined. For example, if galaxies are selected based on luminosity, proper treatments of K-correction and E-correction are required to ensure

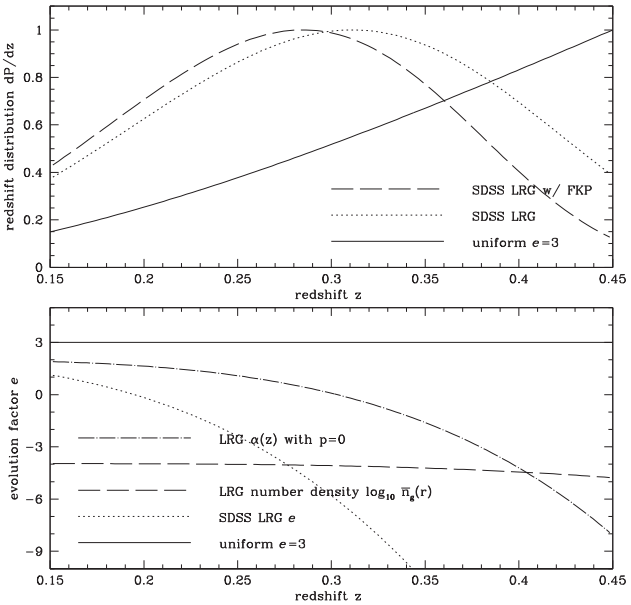

Figure 3. Redshift distribution of the SDSS galaxy sample and the evolution factor e of its number density. In the upper panel, various curves show the normalized redshift distributions (or the radial selection function) in equation (49) for a galaxy sample with a constant comoving number density ($e = 3$: solid) and the SDSS LRG sample (dotted). With the FKP weighting in equation (50), the redshift distribution (dashed) is shifted to lower redshift and is closer to the uniform (solid). The bottom panel shows the evolution factor e of the galaxy number density. By definition, the uniform sample has $e = 3$, diluting only due to the volume expansion. The dotted curve represents the SDSS LRG sample, indicating that its number density evolves rapidly in time (the comoving number density of the SDSS LRG sample is shown as dashed, and the corresponding selection function α is shown as dot–dashed). The galaxy samples in future surveys are assumed to have a uniform distribution ($e = 3$: solid), but with different redshift ranges.

that galaxies are selected by the same luminosity threshold at their rest frame and galaxies in the sample are an identical population over the redshift range. So as to obtain physical insight, we consider idealized situations, in which the comoving galaxy number density is constant ($e = 3$ in equation 41) and the radial selection function is constant ($\alpha = 2$). We refer to these samples as 'uniform' galaxy samples.[4]

We consider three galaxy surveys with the simplified geometry: the SDSS, *Euclid*, and the BigBOSS. While the wide-angle effect in the SDSS is already discussed at length in Samushia et al. (2012) with correct survey geometry, we include the SDSS to set the stage for our calculations of the wide-angle effect in future surveys, as the wide-angle effect is largest in the SDSS among the surveys we consider here.

Fig. 3 describes the redshift distribution of the SDSS galaxy sample and the evolution factor e in equation (41). The redshift distribution $P_z(z)$ is simply the number of expected galaxies at a given redshift bin and is related to the comoving galaxy number density as

$$P_z(z) = \frac{4\pi f_{\rm sky}}{N_{\rm tot}} \frac{r^2}{H} \bar{n}_{\rm g}, \tag{49}$$

where $N_{\rm tot}$ is the total number of observed galaxies, ensuring that the redshift distribution is properly normalized. The redshift distribution of a uniform galaxy sample (solid) in Fig. 3 is skewed to higher redshift due to a larger volume at high redshift. The dotted curve shows the approximate redshift distribution of the SDSS LRG sample (Eisenstein et al. 2001; Cool et al. 2008), and the dashed curve shows the redshift distribution with further FKP weighting (Feldman et al. 1994)

$$w(r) \propto \frac{\bar{n}_{\rm g}}{1 + \bar{n}_{\rm g} P}, \tag{50}$$

where P is the power spectrum at a scale of interest, but is often assumed to be a constant. We adopt $P = 10^4\ (h^{-1}{\rm Mpc})^3$ (e.g. Percival et al. 2010).

The bottom panel shows the evolution factor e in equation (41) and the SDSS LRG number density $\bar{n}_{\rm g}(z)$. The redshift distribution is related to the evolution factor (and hence the selection function) as

$$\frac{{\rm d}\ln P_z}{{\rm d}\ln(1+z)} = 2\frac{1+z}{rH} - \frac{1+z}{H}\frac{{\rm d}H}{{\rm d}z} + (e-3)$$
$$= \frac{1+z}{rH}\left(\alpha - r\frac{{\rm d}H}{{\rm d}z}\right). \tag{51}$$

By construction, a uniform galaxy sample is of $e = 3$ (solid). The dotted curve shows the evolution factor e of the SDSS LRG sample (or the dot–dashed curve for the selection function α), illustrating that non-trivial velocity contributions are present in galaxy clustering due to the evolving population. The mean number density (dashed) of the SDSS LRG sample is about a factor 10 lower at $z = 0.45$ than at the lower boundary in redshift. For *Euclid* and the BigBOSS, we assume uniform galaxy samples (solid curves) but with different redshift ranges.

To quantify the probability distribution of triangle shapes in three galaxy surveys, we create mock catalogues of galaxies by populating the survey region with random particles, and tabulate the probability distribution as a function of triangular configuration (s, μ, Θ) by counting pairs. Figs 4 and 5 describes the probability distribution of the cosine angle μ and the opening angle Θ of the galaxy samples in the SDSS, *Euclid*, and the BigBOSS. The upper panels show the distribution of the cosine angle at a given pair separation, averaged over all pairs with various opening angles. In an idealized situation, the cosine angle of pair separations should be uniformly distributed, as it is nearly so for pairs with small separations (dotted). However, even for a uniform sample, there exist somewhat more pairs along the transverse direction than along the line-of-sight direction simply due to the difference in volume of pairs

$$N^{\parallel}_{\rm pair} \propto \int {\rm d}r \int {\rm d}^2\hat{\boldsymbol{n}}\, \frac{1}{2}\left[\left(r+\frac{s}{2}\right)^2 + \left(r-\frac{s}{2}\right)^2\right], \tag{52}$$

$$N^{\perp}_{\rm pair} \propto \int {\rm d}r \int {\rm d}^2\hat{\boldsymbol{n}}\, r^2 \sin(\theta_{\hat{\boldsymbol{n}}} + \Theta). \tag{53}$$

Therefore, the fractional deviation to the leading order in Θ and s/r is

$$\frac{\Delta N^{\parallel}_{\rm pair}}{N^{\perp}_{\rm pair}} \simeq -\frac{3}{2}\, s\, \frac{\sin\theta_M}{1-\cos\theta_M}\, \frac{r^2_{\rm max} - r^2_{\rm min}}{r^3_{\rm max} - r^3_{\rm min}} \sim -\frac{s}{r_{\rm avg}}\sqrt{\frac{1-f_{\rm sky}}{f_{\rm sky}}}, \tag{54}$$

[4] In literature, a volume-limited galaxy sample is often synonymously used as a uniform sample. However, a volume-limited sample refers to a galaxy sample constructed by imposing a constant luminosity threshold at each redshift (and hence different threshold in observed flux at each redshift), while a uniform galaxy sample simply refers to a galaxy sample with a constant comoving number density. A volume-limited sample can be a uniform sample, but in principle they are unrelated.

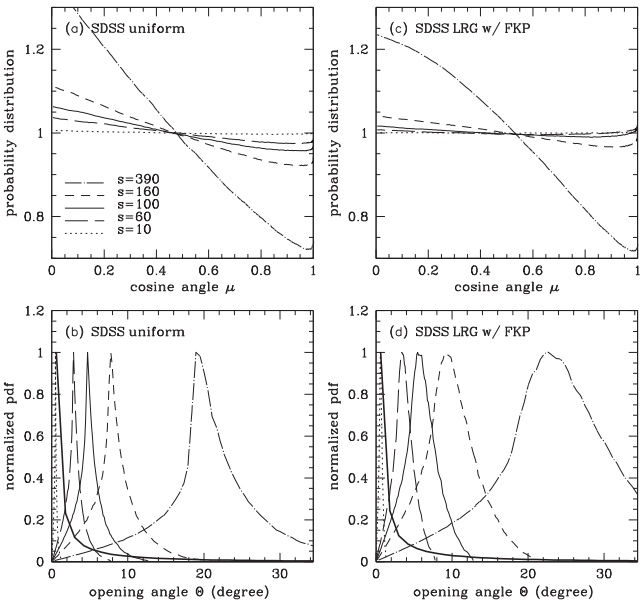

Figure 4. Probability distribution of triangle shapes formed by SDSS galaxy pairs and the observer. Pair distributions are affected by the number density evolution and the survey geometry. For simplicity, the survey geometry is defined in terms of redshift range and sky coverage only; no holes or disjoint regions in the survey areas are assumed. Upper panels show the distribution of the cosine angle between the pair separation vector $\boldsymbol{s}$ and the line-of-sight direction $\hat{\boldsymbol{n}}$ bisecting the pair in angle. Bottom panels show the distribution of the opening angle of galaxy pairs seen by the observer at origin. Various curves represent different separation length $s = |\boldsymbol{s}|$ in units of h^{-1}Mpc. Thick solid curves show the distribution of the opening angle, averaged over all galaxies with any pair separations. With the FKP weighting, more weight is given to galaxies at lower redshift.

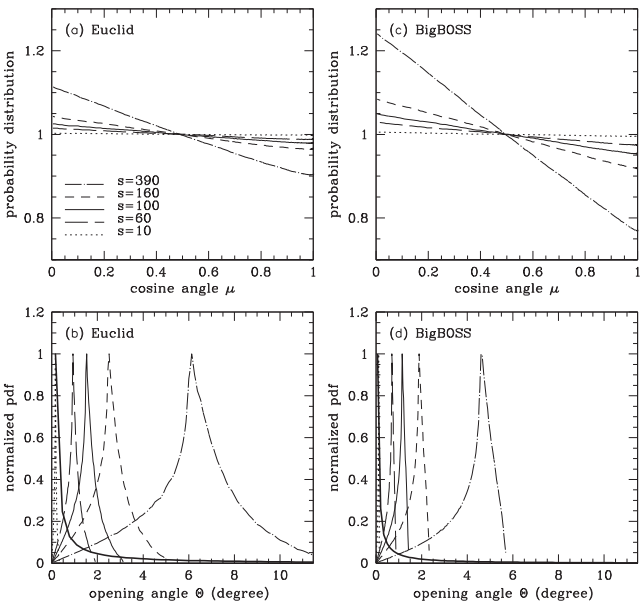

Figure 5. Probability distribution of triangle shapes formed by galaxy pairs and the observer in *Euclid* and the BigBOSS, in the same format as Fig. 4. It is assumed that the sky coverage of *Euclid* is a half ($f_{\rm sky} = 1/2$) and the redshift range is $z = 0.7$–2.0. The BigBOSS is assumed to cover 14 000 deg^2 ($f_{\rm sky} = 0.34$) at $z = 2.2$–3.5. Given the mean distance to galaxy pairs, typical opening angles in these surveys are a lot smaller than in the SDSS. However, the non-uniform distribution of μ is still present, as it is inherent to survey geometry.

where θ_M is the maximum pair separation in angle and ($r_{\rm max}$, $r_{\rm min}$) are the radial distances from the observer, specifying the survey boundary.

The cosine angle μ between the pair separation and the line-of-sight direction is affected by the sky coverage of each survey (including the presence of disjoint regions and holes) and is largely independent of distance to galaxies from the observer. The deviation from the uniform distribution of the cosine angle is proportional to the pair separation, but it also depends on the sky coverage. At larger separation (dot–dashed), the boundary effect becomes more important in determining the probability distribution, as certain triangular shapes cannot fit in the geometry. Consequently, a proper weight should be given to account for the non-uniform distribution of the cosine angle, when measuring the multipole correlation functions or the multipole power spectra (Kazin, Sánchez & Blanton 2012). Compared to the probability distribution in the SDSS in Fig. 4, the μ-distribution in Fig. 5 is more uniform at the same separation in *Euclid* and the BigBoss, reflecting the difference in their sky coverage (*Euclid*: $f_{\rm sky} = 0.5$, BigBOSS: $f_{\rm sky} = 0.34$, SDSS: $f_{\rm sky} = 0.25$).

The bottom panels show the distribution of the opening angle Θ at a given pair separation, averaged over all galaxies with various cosine angle. The distribution of the opening angle Θ is mainly affected by distances to those galaxies from the observer, but it also depends on the sky coverage of each survey. For a galaxy sample with isotropic distribution, the mean cosine angle is $\bar{\mu} = 1/2$, and this configuration, placed at a distance r, would yield an opening angle $\bar{\Theta} \simeq 0.5\, s/r$, when $\Theta \ll 1$. Naturally, the opening angle is close to zero for pairs with small separations (dotted), while it peaks at larger angle for pairs with larger separations (dot–dashed).

The change of the Θ-distribution due to the FKP weighting in Fig. 4 is to broaden the distribution with a slight shift to a larger opening angle, since its effect is largely to pull individual galaxies to lower redshift. Thick solid curves in the bottom panels show the distribution of the opening angle, averaged over all galaxies, not restricted to pair separations. With fewer galaxies at large separation, the average opening angle of galaxy pairs in the SDSS is close to zero (Okumura et al. 2008; Beutler et al. 2011; Samushia et al. 2012). Compared to the probability distribution in the SDSS (Samushia et al. 2012), our probability distribution function in Fig. 4 prefers slightly larger opening angles due to the idealized geometry. The Θ-distribution in Fig. 5 is much smaller than in the SDSS, primarily because galaxy pairs in *Euclid* and the BigBOSS are farther away by a factor of few on average. For pair separations we considered in Fig. 5, the impact of the sky coverage on the Θ-distribution is rather weak in *Euclid* and the BigBOSS. However, the sky coverage or the presence of disjoint regions in practice puts significant constraints on the probability distribution, further reducing the opening angles, as galaxies in two disjoint regions are not used for computing the correlation function.

3.2 Deviation from the simple Kaiser formula with the distant-observer approximation

With the full probability distribution of the triangular configuration formed by galaxy pairs and the observer, we are now ready to compute the full redshift-space correlation function, accounting for the deviation from the simple Kaiser formula with the distant-observer approximation. At a given separation s and a cosine angle μ, there exist a number of galaxy pairs with various opening angle, shown in the bottom panels of Figs 4 and 5. Galaxy pairs that are closer to the observer have larger opening angles at fixed values of s

and μ. For each opening angle Θ available in a given survey region, we use equation (25) to compute the full redshift-space correlation function $\xi_s(s, \phi_1, \phi_2)$, where two angles ϕ_1 and ϕ_2 between the pair separation vector $\boldsymbol{s}$ and two different line-of-sight directions $\hat{\boldsymbol{x}}_1$ and $\hat{\boldsymbol{x}}_2$ are related to the opening angle Θ and the cosine angle μ as

$$\mu = \cos\left(\frac{\phi_1 + \phi_2}{2}\right), \tag{55}$$

$$\Theta = \phi_2 - \phi_1. \tag{56}$$

The triangular configuration is fully specified either by (s, μ, Θ) or by (s, ϕ_1, ϕ_2). The resulting correlation function is then averaged over all galaxy pairs with the same pair separation s and the cosine angle μ as

$$\xi_s(s, \mu) = \frac{\int \mathrm{d}\Theta\, P(\Theta, \mu, s)\, \xi_s(s, \phi_1, \phi_2)}{\int \mathrm{d}\Theta\, P(\Theta, \mu, s)}, \tag{57}$$

where the probability distribution $P(\Theta, \mu, s)$ in the bottom panel of Figs 4 and 5 is proportional to the number of galaxy pairs at a given triangular configuration. We then decompose the resulting correlation function into the redshift–space multipole correlation functions by using

$$\xi_l^s(s) = \frac{2l+1}{2} \int_{-1}^{1} \mathrm{d}\mu\, \mathcal{P}_l(\mu)\, \xi_s(s, \mu). \tag{58}$$

The non-uniform distribution of the cosine angle μ in Figs 4 and 5 prevents from using a simple approach to obtaining the multipole correlation functions:

$$\xi_l^s(s) \neq \frac{2l+1}{2} \frac{\int \mathrm{d}\mu\, \mathcal{P}_l(\mu) \int \mathrm{d}\Theta\, P(\Theta, \mu, s)\, \xi_s(s, \phi_1, \phi_2)}{\int \mathrm{d}\mu \int \mathrm{d}\Theta\, P(\Theta, \mu, s)}. \tag{59}$$

Top panels in Figs 6–8 show the difference of the multipole correlation functions $\xi_l^s(s)$ by using equation (13) with the distant-observer approximation from those obtained by considering the full redshift-space correlation function in equation (57). For simplicity, we assume that the bias factor of the galaxy samples is unity and constant in time. In computing $\xi_l^s(s)$ with the distant-observer approximation, we consider three different cases: mean-redshift (dotted), volume-weighted (dashed), and pair-weighted (solid). As the simplest case (dotted), we compute $\xi_l^s(s)$ by evaluating $P_s(k, \mu_k)$ in equation (6) at the mean redshift, accounting for the change in the logarithmic growth rate f and the growth factor in the matter power spectrum $P_m(k|\bar{z})$. As the next case and a better representation of the measurements, we average the correlation function $\xi_l^s(s)$ with the distant-observer approximation over the survey volume (dashed). As our last case with the highest sophistication (solid), we compute $\xi_l^s(s)$ by evaluating equation (57), but with the full redshift-space correlation function $\xi_s(s, \phi_1, \phi_2)$ replaced by the simple Kaiser formula $\xi_s(s, \mu)$ in equation (12). While the simple Kaiser formula is independent of Θ, we evaluate $\xi_s(s, \mu)$ at the mean redshift of the pair, accounting for the change of pairs at different redshifts.

The three different ways (various curves) of computing $\xi_l^s(s)$ with the distant-observer approximation yield nearly identical results for the SDSS samples in the top panels of Fig. 6. The monopole $\xi_0^s(s)$ becomes negative around $s \sim 130\,h^{-1}$Mpc, while the quadrupole $\xi_2^s(s)$ is negative and the hexadecapole ξ_4^s is positive on all scales. The differences in the multipole correlation functions are $\ll 10^{-3}$ on all scales, which is less than a per cent level of $\xi_l^s(s)$ for $s \leq 200\,h^{-1}$Mpc. However, on large scales $s \gg 200\,h^{-1}$Mpc the correlation function itself is very small, such that the fractional deviation becomes large >10 per cent. Grey curves show the calculation for the SDSS LRG sample with the FKP weighting. No

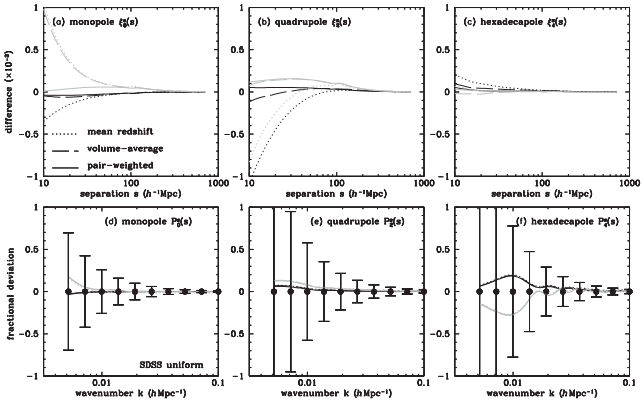

Figure 6. Systematic errors of the simple Kaiser formula with the distant-observer approximation for the SDSS uniform galaxy sample. Grey curves in each panel represent those for the SDSS LRG with the FKP weighting. Top rows show the difference in the multipole correlation functions $\xi_l^s(s)$, and bottom rows show the fractional deviation in the multipole power spectra $P_l^s(k)$. Given a pair separation s and a cosine angle μ, the correlation function is obtained by averaging over all galaxy pairs with different opening angles Θ that fit in the SDSS geometry described in Section 3.1 (equation 57). The multipole correlation functions are obtained by accounting for the non-uniform distribution of the cosine angle μ in Fig. 4, and the multipole power spectra are obtained by Fourier transforming the corresponding multipole correlation functions (see equation 14). Compared to the full redshift-space correlation function, the fractional deviation of the simple Kaiser formula with the distant-observer approximation is obtained in three different ways of evaluation (see text for details): mean-redshift (dotted), volume-averaged (dashed), and pair-weighted (solid). Upper panels: difference in the multipole correlation functions $\xi_0^s(s)$, $\xi_2^s(s)$, and $\xi_4^s(s)$. Bottom panels: fractional deviation of the multipole power spectra $P_0^s(k)$, $P_2^s(k)$, and $P_4^s(k)$. The difference in various curves is largely obscured, as the scales in the bottom panels are vastly different from those in the upper panels. The measurement uncertainties are computed by using the covariance matrix in equation (18), valid in the limit of highly biased objects with negligible shot-noise contribution. The measurement uncertainties are in practice larger and weakly correlated.

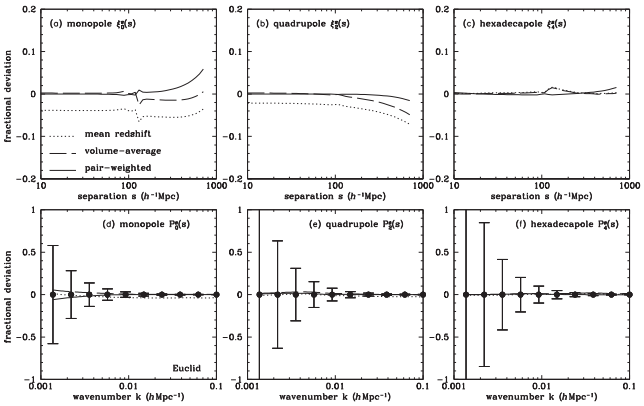

Figure 7. Systematic errors of the simple Kaiser formula with the distant-observer approximation in *Euclid*. Each panel shows the fractional deviation in the multipole correlation function $\xi_l^s(s)$ and the multipole power spectra $P_l^s(k)$. A small but sudden change in $\xi_0^s(s)$ arises at $s \sim 130\,h^{-1}$Mpc when the monopole changes its sign to negative, crossing zero. The survey volume is $V_s = 96\,(h^{-1}\mathrm{Gpc})^3$, approximately 50 times larger than in the SDSS. Correspondingly, the error bars and the minimum wavenumber are smaller. Galaxies in *Euclid* are farther away than in the SDSS. The correlation functions with the distant-observer approximation (dotted) at the mean redshift are off in amplitude, while their shape is still consistent.

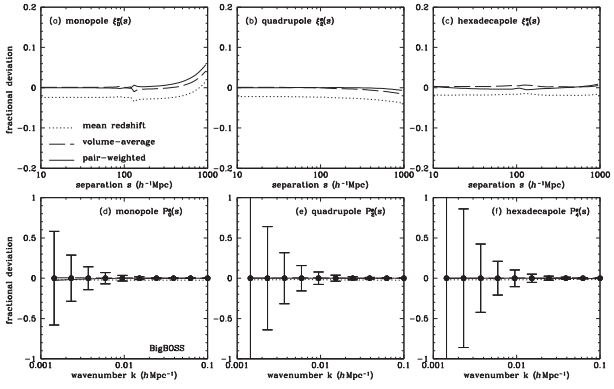

Figure 8. Systematic errors of the simple Kaiser formula with the distant-observer approximation in the BigBOSS, in the same format as Fig. 7. The survey is narrower but deeper than *Euclid*, yielding $V_s = 82\ (h^{-1}\mathrm{Gpc})^3$, similar to *Euclid*. The Kaiser formula is accurate in all practical senses.

substantial difference is present. With the FKP weighting, the mean redshift is reduced to $\bar{z} = 0.27$ from $\bar{z} = 0.34$, and the deviation from the simple Kaiser formula is slightly larger than for the SDSS uniform sample. Since the redshift range of the SDSS is rather narrow $z = 0.15$–0.45, three different ways of computing the simple Kaiser formula with the distant-observer approximation agree well with each other.

Bottom panels of Figs 6–8 quantify the systematic errors in the monopole $P_0^s(k)$, the quadrupole $P_2^s(k)$, and the hexadecapole $P_4^s(k)$ power spectra in the simple Kaiser formula with the distant-observer approximation, where the simple Kaiser formula is again computed by using three different methods (various curves). Using equation (14), the full redshift-space multipole power spectra are computed by Fourier transforming the full redshift–space multipole correlation functions, and the error bars are obtained by using the covariance matrix in equation (18).

The deviation from the distant-observer approximation is again negligible for the SDSS samples on almost all scales (see, also, Samushia et al. 2012). It deviates at most 4 per cent for the monopole and 8 per cent for the quadrupole at the smallest wavenumber available in the survey, while the deviation in the hexadecapole is somewhat larger than in the monopole and the quadrupole due to its sensitivity to larger separation, $s \sim l/k$.

Figs 7 and 8 show the systematic errors of the simple Kaiser formula with the distant-observer approximation in *Euclid* and the BigBOSS. Since galaxies in these surveys are farther away from the observer than in the SDSS, the deviation in the multipole correlation functions at a given separation is even smaller, despite their somewhat larger sky coverage than in the SDSS. In Figs 7 and 8, we now plot the fractional deviations for the multipole correlation functions. With larger redshift ranges in *Euclid* and the BigBOSS, three different ways of computing the simple Kaiser formula start to diverge from each other. The mean redshifts of the surveys are $\bar{z} = 1.4$ and 2.8, and the redshift–space multipole correlation functions at the mean redshift differ from those averaged over the survey volume, because the former evaluates $b^2(\bar{z})D^2(\bar{z})$, $b(\bar{z})f(\bar{z})D^2(\bar{z})$, $f^2(\bar{z})D^2(\bar{z})$ in equations (9)–(11) at the mean redshift, while the latter averages b^2D^2, bfD^2, f^2D^2 over the survey volume, though the difference is less than 10 per cent.

The simplest method (dotted) of computing the multipoles at the mean redshift yields the multipole correlation functions off in amplitude at the 2–4 per cent level on small scales, but the shape is still consistent with the full redshift-space correlation function. The volume-averaged correlation functions (dashed) are better estimates of the full redshift-space correlation function, practically on all scales considered in the plot. While the pair-weighted correlation functions (solid) perform better than the volume-averaged for higher multipoles, the difference is rather small, and it is computationally more expensive, as it needs to be computed for each pair of galaxies. The deviation in the multipole power spectra in the bottom panels are correspondingly small as in the multipole correlation functions in the upper panels. Note again that the scales of the plot in the bottom panels are different from those in the upper panels. With more volume at higher redshifts, these surveys can probe larger scales (smaller k_{min}), and the measurement uncertainties at a fixed scale are substantially reduced by more than a factor of 5. However, as is evident in Figs 7 and 8, the simple Kaiser formula with the distant-observer approximation is in all practical purposes accurate in the future surveys.

3.3 Wide-angle effect in power spectrum analysis

We have discussed the wide-angle effect in the correlation function and the power spectrum measurements in the galaxy surveys. In our comparison, the simple Kaiser formula with the distant-observer approximation is compared to the full redshift-space correlation function in equation (21). However, since no analytic formula accounting for the velocity contribution and the wide-angle effect is available for the redshift-space power spectrum, the deviation in the multiple correlation functions from the simple Kaiser formula is Fourier transformed to compute the deviation in the redshift multipole power spectra. While this procedure should yield the correct result in an ideal case as the correlation function and the power spectrum are Fourier counterparts, the power spectrum analysis in practice is performed in a different way, and these two statistics contain not completely overlapping information as considered only over limited and different ranges of scale.

In general, the power spectrum analysis is performed by using a weighted quadratic function of the observed galaxy number density field, and various methods in the power spectrum analysis differ in how they choose the pair-weighting function (see Tegmark et al. 1998). The standard method including the FKP method is the simplest, in which the weighted number density field $n_{\mathrm{g}}^w(\boldsymbol{s}) = w(\boldsymbol{s})n_{\mathrm{g}}(\boldsymbol{s})$ is Fourier transformed, and their amplitude is an estimate of the redshift-space power spectrum

$$\hat{P}_{\mathrm{s}}(\boldsymbol{k}) \equiv |n_{\mathrm{g}}^w(\boldsymbol{k})|^2 - P_{\mathrm{shot}}(\boldsymbol{k}), \tag{60}$$

where $P_{\mathrm{shot}}(\boldsymbol{k})$ represents the shot-noise contribution. Again, we assume that the shot-noise contribution is negligible.

The FKP method is designed to measure the monopole power spectrum, *not* the anisotropic redshift-space power spectrum.[5] Few

[5] An alternative to this trend has been well developed (Binney & Quinn 1991; Fisher et al. 1994, 1995; Heavens & Taylor 1995; Ballinger, Heavens & Taylor 1995; Hamilton & Culhane 1996), in which the observed galaxy number density is decomposed in terms of radial and angular eigenfunctions of the Helmholtz equation. The analysis is performed on a sphere, explicitly accounting for each line-of-sight direction of galaxies. It forms the most natural basis for all-sky analysis, and it becomes identical to the traditional power spectrum analysis on a small patchy of sky. We refer the reader to the pedagogical review for all-sky likelihood analysis (Hamilton 2005). It has been applied to various galaxy surveys in the past (Fisher et al. 1995; Tadros et al. 1999; Hamilton, Tegmark & Padmanabhan 2000; Taylor et al. 2001; Padmanabhan, Tegmark & Hamilton 2001; Tegmark, Hamilton & Xu 2002; Percival et al. 2004; Tegmark et al. 2004a, 2006; Shapiro, Crittenden

exceptions are Cole et al. (1994) and Yamamoto et al. (2006) analysis of the 2dFGRS. In the former, only pairs in the same but small angular patchy are correlated to ensure that those pairs share the same line-of-sight direction. With this prescription, the power spectrum analysis, however, suffers from non-trivial window function, aliasing of modes, and larger computing cost. No further development or application to observation has been made along this direction. In the latter, a simple method is proposed to account for the line-of-sight direction change in the power spectrum analysis (Yamamoto et al. 2006), while keeping the simplicity in the FKP method. We adopt it to compare the difference among various methods in the power spectrum analysis.

In the standard FKP method, the ensemble average of the power spectrum estimate in equation (60) is

$$\left\langle \hat{P}_{\rm s}(\boldsymbol{k}) \right\rangle = \int {\rm d}^3\boldsymbol{s}_1 \int {\rm d}^3\boldsymbol{s}\, {\rm e}^{-i\boldsymbol{k}\cdot\boldsymbol{s}}\, \bar{n}_{\rm g}^w(\boldsymbol{s}_1)\, \bar{n}_{\rm g}^w(\boldsymbol{s}_2)\, \xi_s(\boldsymbol{s}_1, \boldsymbol{s}_2), \tag{61}$$

where the separation vector is $\boldsymbol{s} = \boldsymbol{s}_1 - \boldsymbol{s}_2$ and the full redshift-space correlation function $\xi_s(\boldsymbol{s}_1, \boldsymbol{s}_2)$ depends on the triangular configuration of the pair, including the opening angle Θ seen from the observer. Since we use the weighted number density $n_{\rm g}^w(\boldsymbol{s})$ rather than the fluctuation $\delta_{\rm g}$, the normalization of the weight function must be chosen to ensure that the power spectrum estimate is unbiased (Feldman et al. 1994),

$$\left\langle \hat{P}_{\rm s}(\boldsymbol{k}) \right\rangle = \int \frac{{\rm d}^3\boldsymbol{k}'}{(2\pi)^3}\, P_{\rm s}(\boldsymbol{k}')\, |\bar{n}_{\rm g}^w(\boldsymbol{k} - \boldsymbol{k}')|^2, \tag{62}$$

and the normalization condition is

$$1 = \int \frac{{\rm d}^3\boldsymbol{k}}{(2\pi)^3} |\bar{n}_{\rm g}^w(\boldsymbol{k})|^2 = \int {\rm d}^3\boldsymbol{s} \left[\bar{n}_{\rm g}^w(\boldsymbol{s})\right]^2. \tag{63}$$

The weighted mean number density $\bar{n}_{\rm g}^w$ is often referred to as the survey window function, and its dimension is $[\bar{n}_{\rm g}^w(\boldsymbol{k})] = V^{1/2}$ and $[\bar{n}_{\rm g}^w(\boldsymbol{s})] = V^{-1/2}$. Fig. 9 delineates the survey window functions. The window functions of four different surveys are largely self-similar, as each survey differs only in the redshift depth and sky coverage. While the survey window function is anisotropic, it can be conveniently decomposed in terms of its multipole functions due to the azimuthal symmetry of the survey geometries we considered in the paper. The monopole (solid) reflects the characteristic scale set by the survey volume, and higher multipoles account for the anisotropy of the survey geometry. When the survey volume is infinite, the monopole becomes the Dirac delta function, and the higher multipoles vanish.

Using equation (8), the multipole power spectra are obtained by angle-averaging the redshift-space power spectrum in equation (61) as

$$\left\langle \hat{P}^s{}_l(k) \right\rangle = (-i)^l (2l+1) \int {\rm d}^3\boldsymbol{s}_1 \int {\rm d}\ln s\, s^3\, j_l(ks) \times \int {\rm d}^2\hat{\boldsymbol{s}}\, \mathcal{P}_l(\hat{\boldsymbol{z}}\cdot\hat{\boldsymbol{s}})\, \bar{n}_{\rm g}^w(\boldsymbol{s}_1)\, \bar{n}_{\rm g}^w(\boldsymbol{s}_2)\, \xi_s(\boldsymbol{s}_1, \boldsymbol{s}_1 - \boldsymbol{s}), \tag{64}$$

& Percival 2012, see also Rassat & Refregier 2012; Pratten & Munshi 2013; Yoo & Desjacques 2013 for recent theoretical development). While the FKP method has been extensively used in recent galaxy surveys (e.g. Percival et al. 2010; Reid et al. 2010), the spherical Fourier analysis provides an alternative, and this method is devoid of any wide-angle effect (hence it is *not* the subject of current investigation). However, the downside of this all-sky analysis is the ambiguity in relating the angular multipole l to the cosine angle μ_k relative to the line-of-sight direction. On small scales, this ambiguity in the correspondence is disadvantageous, as most theoretical models of non-linear redshift-space distortion build on the distant-observer approximation.

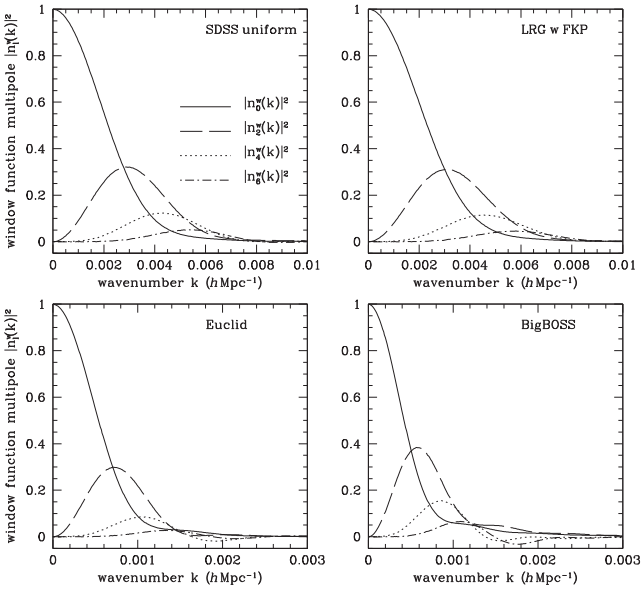

Figure 9. Survey window function multipoles. The survey window function $|n_{\rm g}^w(\boldsymbol{k})|^2$ is decomposed in terms of Legendre polynomials, and only multipoles up to $l = 6$ are plotted. For illustration, the window function is re-normalized to unity at $k = 0$ for the monopole. While the top two panels represent the same survey geometry, their window functions are slightly different due to different weighting scheme.

where the line-of-sight direction is set to be $\hat{\boldsymbol{z}}$-direction and we used

$$\int {\rm d}^2\hat{\boldsymbol{k}}\, {\rm e}^{-i\boldsymbol{k}\cdot\boldsymbol{s}}\, \mathcal{P}_l(\hat{\boldsymbol{n}}\cdot\hat{\boldsymbol{k}}) = 4\pi(-i)^l\, j_l(ks)\, \mathcal{P}_l(\hat{\boldsymbol{n}}\cdot\hat{\boldsymbol{s}}). \tag{65}$$

With the distant-observer approximation, the angular integral in equation (64) becomes

$$\int {\rm d}^2\hat{\boldsymbol{s}}\, \mathcal{P}_l(\hat{\boldsymbol{z}}\cdot\hat{\boldsymbol{s}})\, \xi_s(\boldsymbol{s}_1, \boldsymbol{s}_1 - \boldsymbol{s}) \to \frac{4\pi}{2l+1}\, \xi_l^s(s), \tag{66}$$

and we recover equation (14) for the multipole power spectra $P_l^s(k)$. It becomes clear in equation (64) that the standard FKP method cannot be used to measure the anisotropic redshift-space power spectrum because the line-of-sight direction is fixed as the $\hat{\boldsymbol{z}}$-direction, independent of the pair configuration. This is the reason that the FKP method is used solely for the monopole power spectrum, as is originally intended. However, one issue is that the redshift-space correlation function is Fourier transformed without accounting for the non-uniform distribution of the cosine angle μ.

It is apparent in equation (64) that the redshift-space multipole power spectrum is estimated without accounting for the pair distribution. While the one-point window functions $\bar{n}_{\rm g}^w(\boldsymbol{s}_i)$ are considered, the window function for the pair distribution (or the two-point window function) is not considered in estimating the redshift-space power spectrum. For example, the monopole power spectrum will be estimated by summing all pairs within the survey weighted by the window function, such that it will be biased if the geometry is like a pencil beam, because pairs within the survey are mostly separated along the line-of-sight direction. Naturally, this issue gives rise to negligible systematic errors on small separations compared to the survey scale, but we show in Fig. 10 that it can cause significant systematic errors on large scales.

Due to the simplicity of the FKP method, Yamamoto et al. (2006) attempt to extend the FKP method for the anisotropic redshift-space power spectrum by using a pair-dependent direction

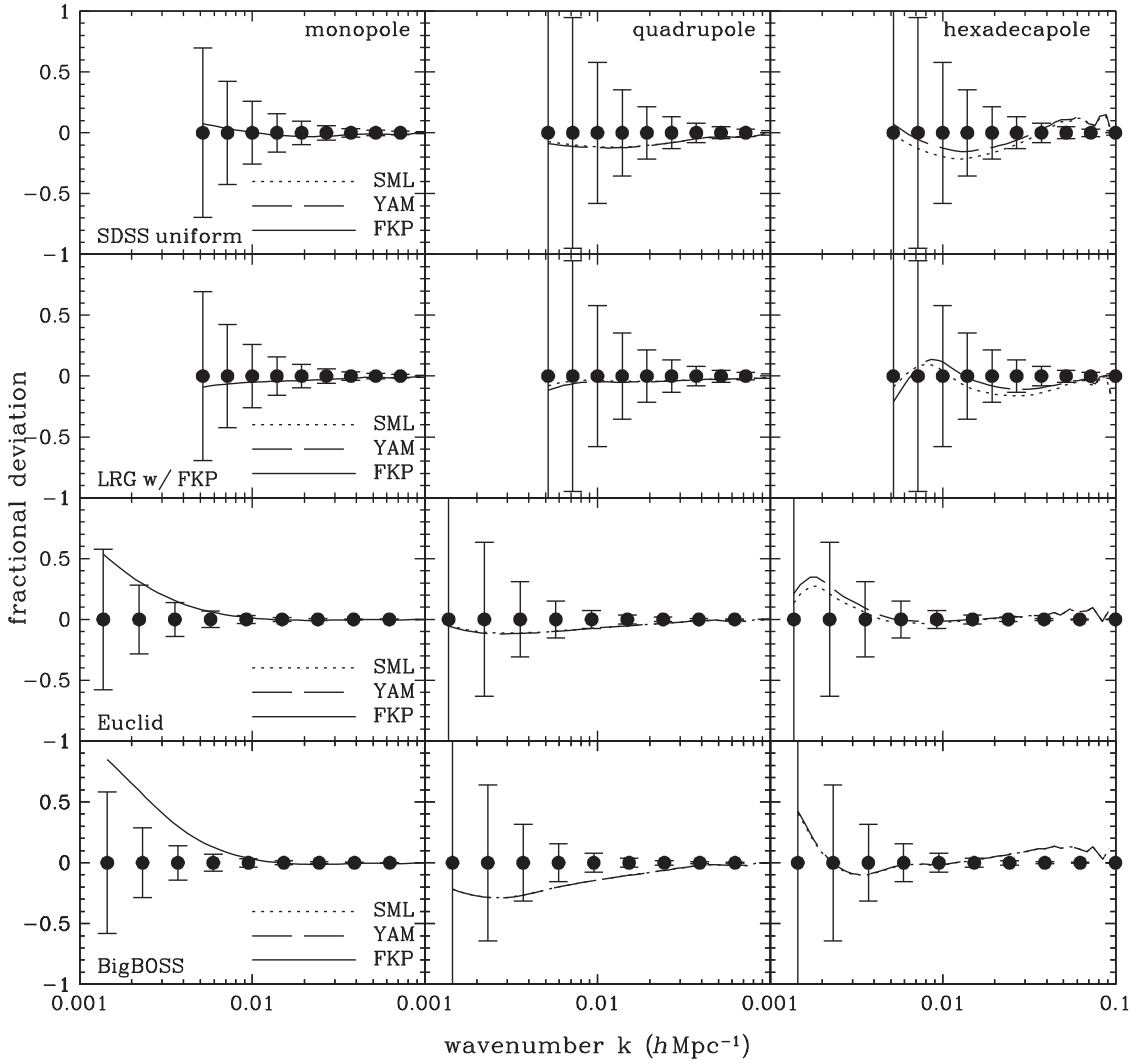

Figure 10. Fractional deviation of estimates of the redshift-space multipole power spectra, relative to the simple Kaiser formula with the distant-observer approximation. All the redshift-space multipole power spectra are scaled by a constant factor to match the monopole on small scales for comparison. Each column shows the monopole, the quadrupole, and the hexadecapoles, and each rows represents four different surveys. The multipole power spectra with the distant-observer approximation are volume-averaged over the survey volume and convolved with the survey window function. Three different curves represent different estimates of the redshift-space multipole power spectra. While these estimators differ only in defining the line-of-sight direction for galaxy pairs (FKP, Feldman et al. 1994; YAM, Yamamoto et al. 2006; SML, Szalay et al. 1998), they are identical for the monopole power spectrum, and two methods (YAM and SML) yield similar results for higher multipoles, as their line-of-sight directions are nearly identical due to large distances to galaxy pairs in surveys.

$\boldsymbol{s}_h \equiv (\boldsymbol{s}_1 + \boldsymbol{s}_2)/2$ as the line-of-sight direction for each pair, such that the estimators for the redshift-space multipole power spectra are

$$\hat{P}_l^{\rm Y}(\boldsymbol{k}) \equiv \int {\rm d}^3\boldsymbol{s}_1 \int {\rm d}^3\boldsymbol{s}\, {\rm e}^{-{\rm i}\boldsymbol{k}\cdot\boldsymbol{s}}\, n_{\rm g}^w(\boldsymbol{s}_1)\, n_{\rm g}^w(\boldsymbol{s}_2)\, \mathcal{P}_l(\hat{\boldsymbol{s}}_h \cdot \hat{\boldsymbol{k}}). \quad (67)$$

Their ensemble averages are

$$\left\langle \hat{P}_l^{\rm Y}(k) \right\rangle = (-i)^l (2l+1) \int {\rm d}^3\boldsymbol{s}_1 \int {\rm d}\ln s\, s^3 j_l(ks) \times \int {\rm d}^2\hat{\boldsymbol{s}}\, \mathcal{P}_l(\hat{\boldsymbol{s}}_h \cdot \hat{\boldsymbol{s}}) \bar{n}_{\rm g}^w(\boldsymbol{s}_1)\, \bar{n}_{\rm g}^w(\boldsymbol{s}_2)\, \xi_s(\boldsymbol{s}_1, \boldsymbol{s}_1 - \boldsymbol{s}), \quad (68)$$

and we recover the same limit with the distant-observer approximation. As opposed to the standard FKP method, the Yamamoto method is computationally more expensive, because one cannot simply Fourier transform the weighted number density $n_{\rm g}^w$ and compute its amplitude to estimate the redshift-space multipole power spectrum, instead it has to be estimated by a pair-dependent way. As another way of measuring the redshift-space multipole power spectra, we also consider a variant of the Yamamoto method by using the line-of-sight direction $\hat{\boldsymbol{n}}$ that bisects the pair in angle (see Fig. 1). All of the three FKP-based methods agree for the monopole power spectrum, as the angle average of the wavevector removes the need to define the line-of-sight direction, and as is intended in the original FKP method. Regarding the non-uniform distribution of cosine angle μ, this issue is not addressed in any of the three methods for measuring the redshift-space multipole power spectra, and we find that substantial systematic errors arise from this issue in future surveys.

Fig. 10 compares the three different estimates of the redshift-space multipole power spectra to the simple Kaiser formula with the distant-observer approximation. We compute the redshift-space multipole power spectra for each method by generating random catalogues of galaxies and by considering a spherical volume integral

of the full redshift-space correlation function $\xi_s(\boldsymbol{s}_1, \boldsymbol{s}_2)$ in equations (64) and (68) from each galaxy in the catalogues. For comparison, we obtain the theoretical prediction by convolving the simple Kaiser formula at the mean redshift with the survey window function as in equation (62). Four different surveys are displayed in four rows, and the redshift-space multipole power spectra are presented in three columns.

In the previous section, the redshift-space correlation function is averaged over the different opening angle Θ, the multipole correlation functions $\xi_l^s(s)$ are then obtained by accounting for the non-uniform distribution of cosine angle μ, and they are finally Fourier transformed to obtain the redshift-space multipole power spectra $P_l^s(k)$. However, in equation (61), the power spectrum receives contributions with equal weight from all the correlation function at a given (s, μ) but with different opening angle Θ, which will change the normalization even on smallest scales, where the distant-observer approximation is accurate. Therefore, we scale the monopole power spectrum estimate with a constant factor to match the convolved monopole power spectrum with the distant-observer approximation at $k = 0.1\,h\,\mathrm{Mpc}^{-1}$, but the same scale factor is used to scale the quadrupole and the hexadecapole power spectra. These scale factors result in 10–20 per cent shifts in amplitude for each survey, but they can be absorbed into unknown galaxy bias factor.

The left-hand column shows the monopole power spectrum for each survey, and the three different methods yield identical results for the monopole. The deviation of the monopole estimates in the SDSS is negligible, compared to the sample variance, and the simple Kaiser formula with the distant-observer approximation provides a good approximation to the monopole power spectrum measurement. As galaxies in *Euclid* and the BigBOSS are farther away than in the SDSS, the wide-angle effect becomes irrelevant in these surveys. However, while the survey volume in *Euclid* and the BigBOSS is dramatically larger than in the SDSS, the sky coverage increases only a little, especially so in the BigBOSS. This affects the distribution of cosine angle μ at the largest separations, and the deviation in the monopole power spectrum is larger than the sample variance, a potential systematic error that needs to be addressed in the future surveys.

The middle and the right-hand columns show the quadrupole and the hexadecapole power spectra. Note that the standard FKP method is not intended to measure the anisotropic redshift-space power spectrum.[6] Two methods correctly define the line-of-sight direction for each galaxy pair and yield virtually identical results for the quadrupole and the hexadecapole. As opposed to the monopole power spectrum, where the deviations accumulate, the effect of the non-uniform distribution of μ is smaller for the quadrupole and the hexadecapole, as the higher order Legendre polynomials oscillate around zero. There exist small but wiggly deviations on small scales for the hexadecapole power spectrum. On those scales, the distant-observer approximation is accurate and the μ-distribution is uniform. We suspect that the few per cent level deviations on small scales are numerical artefact, arising from the complication of multidimensional integration in equation (62) and the sensitivity to angular structure in the survey window function.

[6] Blake et al. (2011a) measured the WiggleZ redshift-space power spectrum by using both the standard FKP and the Yamamoto methods. Although no significant detection is made for the hexadecapole power spectrum $P_4(k)$ in the WiggleZ survey, they find that both methods yield measurements of the monopole and the quadrupole power spectra, consistent with each other. While the sky coverage in the WiggleZ survey is $\sim$1000 deg^2, it is divided into six disjoint regions, each of which is subtended by $\sim$10 deg. Therefore, as noted in Blake et al. (2011a), a single line-of-sight assignment to all galaxies in each region is a good approximation in the WiggleZ survey.

4 DISCUSSION

We have investigated the wide-angle effects in galaxy clustering measurements in galaxy surveys such as the SDSS, *Euclid* and the BigBOSS. We have found that compared to the measurement uncertainties associated with the redshift–space multipole correlation functions the wide–angle effects are negligible in the SDSS (as discussed in Samushia et al. 2012) and they are completely irrelevant in the future surveys, provided that the Kaiser formula is averaged over the survey volume to represent the redshift-space correlation function at the representative redshift. While we have reached the same conclusion in the power spectrum analysis, the standard power spectrum analysis based on the FKP method is performed in a slightly different way, carrying a systematic flaw that can result in substantial systematic errors in the future surveys. Furthermore, we have clarified a connection of the Kaiser formula to the relativistic formula of galaxy clustering, and have found corrections to the formula often used for computing the correlation function of widely separated pairs.

In literature, the 'wide angle effects' are often used to refer to the deviation from the simple Kaiser formula with the distant-observer approximation, but they arise owing to two physically distinct effects. First, the two-point correlation function involves a triangle formed by a galaxy pair and the observer, and the triangle is described by two line-of-sight directions and the pair separation. The two line-of-sight directions of each galaxy deviate from the one and only line-of-sight direction in the distant-observer approximation, and the resulting correlation function depends on the triangular configuration, whereas the simple Kaiser formula is just a function of the pair separation and the angle it makes with the line-of-sight direction. This effect is legitimately called the wide-angle effect. The other effect that contributes to the deviation from the simple Kaiser formula is the velocity contribution to galaxy clustering in redshift-space. Even in linear theory, the velocity terms are present in the full Kaiser formula, arising from the mapping of galaxy number densities in real-space to redshift-space. Moreover, the relativistic treatment of galaxy clustering reveals the presence of the gravitational potential contribution to galaxy clustering, though their corrections are even smaller than the velocity contribution. This effect is often referred to as the wide-angle effect, but is independent of how widely galaxy pairs are separated on the sky.

We have made a connection of the full Kaiser formula to the relativistic description of galaxy clustering (Yoo et al. 2012). The full Kaiser formula is valid up to the velocity contribution, only when galaxy samples are selected without any bias, except one from the observed redshift. Furthermore, we have found that even the full Kaiser formula is not properly considered in the formula for computing the redshift-space correlation function (Szalay et al. 1998; Szapudi 2004; Pápai & Szapudi 2008). In light of the relativistic treatment, the derivative in the Jacobian mapping to redshift-space involves the time derivative as well as the spatial derivative, as we only observe galaxies in the past light cone. The (missing) time derivative give corrections to the velocity contribution. While these terms again contribute to negligible systematic errors, they can be readily implemented to the existing formula by modifying the selection function α (see, Section 2.4 for details).

The main reason that the deviation from the distant-observer approximation is small is already evident in Fig. 2: Galaxies in typical surveys are substantially far away from the observer, and

there are simply *not* many galaxies in the local neighbourhood, where the opening angles of galaxy pairs can be large. For example, typical galaxy pairs at a separation $s \simeq 100\,h^{-1}$Mpc in the SDSS would appear subtended by less than 5 deg on the sky, and this trend is accelerated in future surveys at higher redshifts, where typical distances to galaxy samples in those surveys are at least twice larger than in the SDSS. A similar argument can be made to attempt to reach the opposite conclusion: given a typical distance r to galaxy pairs in a survey, the deviation from the distant-observer approximation becomes substantial as widely separated galaxy pairs are considered. This argument is in fact true, and non-negligible deviations (>10 per cent) in the multipole correlation functions in Fig. 6 exist at $s > 400\,h^{-1}$Mpc, while the deviations in future surveys at higher redshifts are substantially smaller (see, Figs 7 and 8). However, the deviations are smaller than one naively expects: at a given pair separation s and cosine angle μ, the correlation function $\xi_s(s, \mu)$ is obtained by averaging the full correlation function $\xi_s(s, \mu, \Theta)$ over all galaxy pairs with different opening angles Θ. With more volume at a larger distance from the observer, the correlation function is skewed to that of galaxy pairs farther away from the observer, of which the opening angles are smaller.

However small, the deviations may matter in the era of precision cosmology. To quantify the systematic errors associated with the distant-observer approximation, we have computed the covariance matrix of the redshift-space multipole power spectra, obtained by Fourier transforming the redshift–space multipole correlation functions, accounting for the deviation from the distant-observer approximation. In agreement with Samushia et al. (2012), we have found that the systematic errors by using the distant-observer approximation are negligible in the SDSS on all scales (see Fig. 6), provided that the Kaiser formula with the distant-observer approximation is properly evaluated. It is found that averaging the prediction of the Kaiser formula over the survey volume yields the best match to the full redshift-space clustering measurements, while the evaluation at the mean redshift of the survey would be just fine at the few per cent level in amplitude (the shape is correctly estimated in both cases). Furthermore, this conclusion remains valid in future surveys such as *Euclid* and the BigBOSS at higher redshifts (Figs 7 and 8). At a given pair separation (with fixed sky coverage), one would need a survey at a higher redshift to reduce measurement uncertainties associated with that scale by sampling more independent Fourier modes, $\sigma \propto 1/\sqrt{N_k} \propto 1/\sqrt{V} \propto 1/r$. However, since the deviation from the distant-observer approximation is to the least, $\sin\Theta \simeq \Theta \propto 1/r$ or $|\cos\Theta - 1| \simeq \Theta^2 \propto 1/r^2$, the systematic errors in the distant-observer approximation can only decrease in a survey at higher redshifts, and they are already negligible in the SDSS.

While the distant-observer approximation is accurate in those surveys, the power spectrum measurements have an issue in the standard power spectrum analysis. Although negligible in the SDSS, we have found that the non-uniform distribution of cosine angle μ between the line-of-sight and the pair separation directions is *not* properly considered in the standard power spectrum analysis and can be a substantial source of systematic errors in the future surveys (see Fig. 10).

Our conclusion should be taken with caution that systematic errors incurred by adopting the distant-observer approximation for computing the redshift-space galaxy clustering are negligible in generic galaxy redshift surveys such as the SDSS, *Euclid*, and the BigBOSS, provided that the correlation function or the power spectrum is obtained by properly averaging over all galaxy pairs in the surveys. Certainly, one could divide survey regions into multiple redshift bins with narrow width to prevent further dilution of the correlation function or the power spectrum due to averaging over galaxy pairs at farther distances (see e.g. Asorey et al. 2012; Montanari & Durrer 2012). However, it still remains to be demonstrated whether the systematic errors of the distant-observer approximation in those survey configurations can be important, because smaller volumes in those redshift bins lead to larger measurement uncertainties.

Alternatively, instead of using the currently popular methods discussed in this paper, one can choose to use the maximum likelihood methods and measure the correlation function $\xi_s(s, \phi_1, \phi_2)$ or the spherical power spectrum based on spherical Fourier decomposition (e.g. Fisher et al. 1994; Heavens & Taylor 1995; Tegmark et al. 2004b; Hamilton 2005). Under the approximation that the underlying distribution is Gaussian, this will circumvent the issues of the wide-angle effect and the non-uniform distribution on large scales. Further decomposition into the standard redshift-space multipole correlation function $\xi_l^s(s)$ or power spectrum $P_l^s(k)$ would require the assumption that the observed correlation function or spherical power spectrum be well described by the simple Kaiser formula with the distant-observer approximation, which we showed is a good approximation. We suspect that maximum likelihood methods may provide optimal ways to measure large-scale clustering without significant issues discussed in this paper.

ACKNOWLEDGEMENTS

We acknowledge useful discussions with Florian Beutler, Eyal Kazin, Shun Saito, Anze Slosar, and Martin White. This work is supported by the Swiss National Foundation (SNF) under contract 200021-116696/1 and WCU grant R32-10130. JY is supported by the SNF Ambizione Grant.

REFERENCES

Asorey J., Crocce M., Gaztañaga E., Lewis A., 2012, MNRAS, 427, 1891
Ballinger W. E., Heavens A. F., Taylor A. N., 1995, MNRAS, 276, L59
Bertacca D., Maartens R., Raccanelli A., Clarkson C., 2012, J. Cosmol. Astropart. Phys., 10, 25
Beutler F. et al., 2011, MNRAS, 416, 3017
Binney J., Quinn T., 1991, MNRAS, 249, 678
Blake C. et al., 2010, MNRAS, 406, 803
Blake C. et al., 2011a, MNRAS, 415, 2876
Blake C. et al., 2011b, MNRAS, 415, 2892
Bonvin C., Durrer R., 2011, Phys. Rev. D, 84, 063505
Challinor A., Lewis A., 2011, Phys. Rev. D, 84, 043516
Cole S., Fisher K. B., Weinberg D. H., 1994, MNRAS, 267, 785
Cole S. et al., 2005, MNRAS, 362, 505
Colless M. et al., 2001, MNRAS, 328, 1039
Cool R. J. et al., 2008, ApJ, 682, 919
Drinkwater M. J. et al., 2010, MNRAS, 401, 1429
Eisenstein D. J. et al., 2001, AJ, 122, 2267
Eisenstein D. J. et al., 2005, ApJ, 633, 560
Feldman H. A., Kaiser N., Peacock J. A., 1994, ApJ, 426, 23
Fisher K. B., Scharf C. A., Lahav O., 1994, MNRAS, 266, 219
Fisher K. B., Lahav O., Hoffman Y., Lynden-Bell D., Zaroubi S., 1995, MNRAS, 272, 885
Hamilton A. J. S., 1992, ApJ, 385, L5
Hamilton A. J. S., 2005, in Martinez V., ed., Data Analysis in Cosmology
Hamilton A. J. S., Culhane M., 1996, MNRAS, 278, 73
Hamilton A. J. S., Tegmark M., Padmanabhan N., 2000, MNRAS, 317, L23
Heavens A. F., Taylor A. N., 1995, MNRAS, 275, 483
Jeong D., Schmidt F., Hirata C. M., 2012, Phys. Rev. D, 85, 023504
Kaiser N., 1984, ApJ, 284, L9
Kaiser N., 1987, MNRAS, 227, 1

Kazin E. A., Sánchez A. G., Blanton M. R., 2012, MNRAS, 419, 3223
Lynden-Bell D., 1971, MNRAS, 155, 95
Matsubara T., 2000, ApJ, 535, 1
Meiksin A., White M., 1999, MNRAS, 308, 1179
Montanari F., Durrer R., 2012, Phys. Rev. D, 86, 063503
Okumura T., Matsubara T., Eisenstein D. J., Kayo I., Hikage C., Szalay A. S., Schneider D. P., 2008, ApJ, 676, 889
Padmanabhan N., Tegmark M., Hamilton A. J. S., 2001, ApJ, 550, 52
Pápai P., Szapudi I., 2008, MNRAS, 389, 292
Peebles P. J. E., 1980, The Large-scale Structure of the Universe. Princeton Univ. Press, Princeton, NJ
Percival W. J. et al., 2004, MNRAS, 353, 1201
Percival W. J. et al., 2010, MNRAS, 401, 2148
Pratten G., Munshi D., 2013, MNRAS, 436, 3792
Raccanelli A., Samushia L., Percival W. J., 2010, MNRAS, 409, 1525
Raccanelli A. et al., 2013, MNRAS, 436, 89
Rassat A., Refregier A., 2012, A&A, 540, A115
Reid B. A. et al., 2010, MNRAS, 404, 60
Sachs R. K., Wolfe A. M., 1967, ApJ, 147, 73
Samushia L., Percival W. J., Raccanelli A., 2012, MNRAS, 420, 2102
Sánchez A. G. et al., 2012, MNRAS, 425, 415
Schlegel D. J. et al., 2007, in American Astronomical Society Meeting Abstracts Vol. 211, SDSS-III: The Baryon Oscillation Spectroscopic Survey (BOSS). Am. Astron. Soc., Washington, DC, p. 132.29
Shapiro C., Crittenden R. G., Percival W. J., 2012, MNRAS, 422, 2341
Szalay A. S., Matsubara T., Landy S. D., 1998, ApJ, 498, L1
Szapudi I., 2004, ApJ, 614, 51
Tadros H. et al., 1999, MNRAS, 305, 527
Taruya A., Nishimichi T., Saito S., 2010, Phys. Rev. D, 82, 063522
Taylor A. N., Ballinger W. E., Heavens A. F., Tadros H., 2001, MNRAS, 327, 689
Tegmark M., Hamilton A. J. S., Strauss M. A., Vogeley M. S., Szalay A. S., 1998, ApJ, 499, 555
Tegmark M., Hamilton A. J. S., Xu Y., 2002, MNRAS, 335, 887
Tegmark M. et al., 2004a, Phys. Rev. D, 69, 103501
Tegmark M. et al., 2004b, ApJ, 606, 702
Tegmark M. et al., 2006, Phys. Rev. D, 74, 123507
Yamamoto K., Nakamichi M., Kamino A., Bassett B. A., Nishioka H., 2006, PASJ, 58, 93
Yoo J., 2009, Phys. Rev. D, 79, 023517
Yoo J., 2010, Phys. Rev. D, 82, 083508
Yoo J., Desjacques V., 2013, Phys. Rev. D, 88, 023502
Yoo J., Fitzpatrick A. L., Zaldarriaga M., 2009, Phys. Rev. D, 80, 083514
Yoo J., Hamaus N., Seljak U., Zaldarriaga M., 2012, Phys. Rev. D, 86, 063514
York D. G. et al., 2000, AJ, 120, 1579

APPENDIX A: COVARIANCE MATRIX OF MULTIPOLE POWER SPECTRA

With the distant-observer approximation, the redshift-space power spectrum is well described by the simple Kaiser formula in equation (6) in the linear regime, and it consists of only three multipole power spectra. While the covariance matrix of the multipole power spectra is diagonal in Fourier modes $\propto\delta_{kk'}$, they are correlated between different angular multipoles. Using equation (17), the diagonal components of the covariance matrix can be computed as

$$\begin{aligned}\mathrm{Cov}\left[\hat{P}^s{}_0\hat{P}^s{}_0\right] &= \left[\tilde{P}^s{}_0\right]^2+\frac{1}{5}\left[P_2^s\right]^2+\frac{1}{9}\left[P_4^s\right]^2\\ &= \frac{1}{\bar{n}_{\rm g}^2}+\frac{2}{\bar{n}_{\rm g}}\left(1+\frac{2\beta}{3}+\frac{\beta^2}{5}\right)b^2P_m\\ &\quad+\left(1+\frac{4\beta}{3}+\frac{6\beta^2}{5}+\frac{4\beta^3}{7}+\frac{\beta^4}{9}\right)\left[b^2P_m\right]^2,\end{aligned}\tag{A1}$$

$$\begin{aligned}\mathrm{Cov}\left[\hat{P}^s{}_2\hat{P}^s{}_2\right] &= 5\left[\tilde{P}^s{}_0\right]^2+\frac{20}{7}\tilde{P}^s{}_0P_2^s+\frac{15}{7}\left[P_2^s\right]^2+\frac{20}{7}\tilde{P}^s{}_0P_4^s\\ &\quad+\frac{120}{77}P_2^sP_4^s+\frac{8945}{9009}\left[P_4^s\right]^2\\ &= \frac{5}{\bar{n}_{\rm g}^2}+\frac{10}{\bar{n}_{\rm g}}\left(1+\frac{22\beta}{21}+\frac{3\beta^2}{7}\right)b^2P_m\\ &\quad+5\left(1+\frac{44\beta}{21}+\frac{18\beta^2}{7}+\frac{340\beta^3}{231}+\frac{415\beta^4}{1287}\right)\\ &\quad\times\left[b^2P_m\right]^2,\end{aligned}\tag{A2}$$

$$\begin{aligned}\mathrm{Cov}\left[\hat{P}^s{}_4\hat{P}^s{}_4\right] &= 9\left[\tilde{P}^s{}_0\right]^2+\frac{360}{77}\tilde{P}^s{}_0P_2^s+\frac{16101}{5005}\left[P_2^s\right]^2\\ &\quad+\frac{2916}{1001}\tilde{P}^s{}_0P_4^s+\frac{3240}{1001}P_2^sP_4^s+\frac{42849}{17017}\left[P_4^s\right]^2\\ &= \frac{9}{\bar{n}_{\rm g}^2}+\frac{18}{\bar{n}_{\rm g}}\left(1+\frac{78\beta}{77}+\frac{1929\beta^2}{5005}\right)b^2P_m\end{aligned}\tag{A3}$$

$$+9\left(1+\frac{156\beta}{77}+\frac{11574\beta^2}{5005}+\frac{1308\beta^3}{1001}+\frac{711\beta^4}{2431}\right)\left[b^2P_m\right]^2,\tag{A4}$$

where $\tilde{P}^s{}_0\equiv P_0^s+1/\bar{n}_{\rm g}$ and we suppressed the scale-dependence of the multipole power spectra and their covariance matrix. In Taruya et al. (2010), there were minor typos in their equation (C4) for Cov$[\hat{P}^s{}_2\hat{P}^s{}_2]$. The off-diagonal components of the covariance matrix are

$$\begin{aligned}\mathrm{Cov}\left[\hat{P}^s{}_0\hat{P}^s{}_2\right] &= 2\tilde{P}^s{}_0P_2^s+\frac{2}{7}\left[P_2^s\right]^2+\frac{4}{7}P_2^sP_4^s+\frac{100}{693}\left[P_4^s\right]^2\\ &= \frac{8\beta}{\bar{n}_{\rm g}}\left(\frac{1}{3}+\frac{\beta}{7}\right)b^2P_m\\ &\quad+8\beta\left(\frac{1}{3}+\frac{3\beta}{7}+\frac{5\beta^2}{21}+\frac{5\beta^3}{99}\right)\left[b^2P_m\right]^2,\end{aligned}\tag{A5}$$

$$\begin{aligned}\mathrm{Cov}\left[\hat{P}^s{}_0\hat{P}^s{}_4\right] &= \frac{18}{35}\left[P_2^s\right]^2+2\tilde{P}^s{}_0P_4^s+\frac{40}{77}P_2^sP_4^s+\frac{162}{1001}\left[P_4^s\right]^2\\ &= \frac{16\beta^2}{35\bar{n}_{\rm g}}b^2P_m+48\beta^2\left(\frac{1}{35}+\frac{2\beta}{77}+\frac{\beta^2}{143}\right)\\ &\quad\times\left[b^2P_m\right]^2,\end{aligned}\tag{A6}$$

$$\begin{aligned}\mathrm{Cov}\left[\hat{P}^s{}_2\hat{P}^s{}_4\right] &= \frac{36}{7}\tilde{P}^s{}_0P_2^s+\frac{108}{77}\left[P_2^s\right]^2+\frac{200}{77}\tilde{P}^s{}_0P_4^s\\ &\quad+\frac{3578}{1001}P_2^sP_4^s+\frac{900}{1001}\left[P_4^s\right]^2\\ &= \left(\frac{48\beta}{7\bar{n}_{\rm g}}+\frac{272\beta^2}{77\bar{n}_{\rm g}}\right)b^2P_m\\ &\quad+\left(\frac{48\beta}{7}+\frac{816\beta^2}{77}+\frac{6960\beta^3}{1001}+\frac{240\beta^4}{143}\right)\\ &\quad\times\left[b^2P_m\right]^2.\end{aligned}\tag{A7}$$

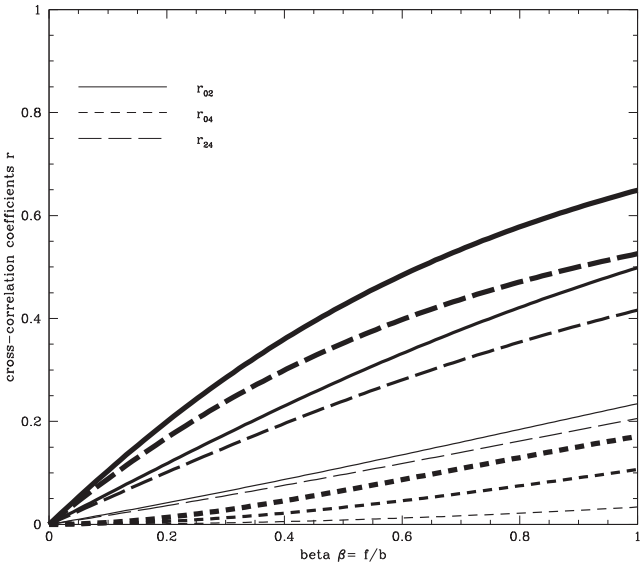

Figure A1. Cross-correlation of the multipole covariance matrices. As a function of $\beta = f/b$, various curves show the cross-correlation coefficients r_{02} (solid), r_{04} (dashed), r_{24} (short dashed). With increasing thickness, each curve represents galaxy samples with $\bar{n}_g P_g = 0.2$ (thin), 1 (thicker), and 10 (thickest).

The degree to which the covariance matrix of the multipole power spectra is correlated is described by the cross-correlation coefficients:

$$r_{l_1 l_2} = \frac{\mathrm{Cov}\left[\hat{P}^s_{l_1}\hat{P}^s_{l_2}\right]}{\sqrt{\mathrm{Cov}\left[\hat{P}^s_{l_1}\hat{P}^s_{l_1}\right]\ \mathrm{Cov}\left[\hat{P}^s_{l_2}\hat{P}^s_{l_2}\right]}}, \tag{A8}$$

ranges from zero (uncorrelated) to unity (perfectly correlated). Fig. A1 shows the cross-correlation coefficients. Three different curves show the coefficients r_{02} (solid), r_{04} (dashed), and r_{24} (short dashed), respectively. For each curve, there exist three different thickness, by which three ratios of the sample variance to the shot noise are considered. Throughout the paper, we considered the sample variance limited case $\bar{n}_g P_g = \infty$, in which the galaxy number density is high and the shot noise contribution is negligible. The cases with $\bar{n}_g P_g = 10$ (thickest), 1 (thicker), and 0.2 (thin) approximately correspond to the SDSS LRG sample at $k = 0.01$, 0.15, and $0.3\,h\,\mathrm{Mpc}^{-1}$, respectively. All of three cases show that the covariance matrix becomes uncorrelated in the limit of highly biased galaxy sample ($\beta \to 0$).

This paper has been typeset from a TEX/LATEX file prepared by the author.